3D SEISMIC ANALYSIS OF CENOZOIC SLOPE DEPOSITS AND FLUID FLOW PHENOMENA ALONG THE NIGERIAN TRANSFORM MARGIN

Oluwatobi Olobayo [1,2] & Mads Huuse [2]

[1] Data, Digital and Technology Limited, UK (tobi@datadigitalandtechnologylimited.com)

[2] The University of Manchester, Manchester M13 9 PL, England, UK (mads.huuse@manchester.ac.uk)

ABSTRACT

3D seismic data provide new insights on ~ 2 km thick Cenozoic post-transform slope sediments and fluid-flow phenomena along the Nigerian Transform Margin. The study documents large-scale mass-transport deposits (MTDs), deep-water channels, sediment waves, and a range of fluid flow phenomena such as pockmarks, pipes, seabed mound and gas-hydrates. They are observed from Pliocene-aged sediments and distributed above structural highs, regional faults and active and relic deep-water channels in the eastern part of the area, closest to the Niger Delta cone. The fluid flow features are interpreted to be indicative of an active petroleum system in the deeper subsurface, and from fluid migration along planes of deep-seated faults. MTDs are mapped at multiple levels and the volume of failed sediments increased through time within the western part of the study area. The repeated and increased volume of MTDs in the area is attributed to an increased rate of sedimentation through time and slope gradient during the late Cenozoic. The presence of repeated MTDs and fluid flow phenomena on the Nigerian Transform Margin has implications for installations of offshore facilities as they constitute potential geohazards. The study also documents, for the first time, polygonal fault systems offshore Nigeria.

1 INTRODUCTION

Significant interest and exploration activity along the equatorial conjugate margins led to acquisition of a 2,845 km^2 high-resolution 3D reflection seismic ('Geostreamer') data from the Nigeria Transform Margin in 2010 by Petroleum Geo-Services (PGS) in cooperation with the Nigerian Upstream Petroleum Regulatory Commission (NUPRC). It was acquired, to confirm the presence of Cretaceous play fairways already discovered along the West African Transform and Brazilian margins (Fig. 1). The survey area falls within the Dahomey-Benin basin, part of the east-west aligned sedimentary basins formed during Late Cretaceous rifting of the African and South American plates (Brownfield & Charpentier 2006; Greenhalgh *et al.,* 2011) and of major interest due to the hydrocarbon exploration potentials realised from the Aje field and Ogo discovery, making this study relevant to exploration. Hydrocarbon generation within the basin began in the Late Miocene and continues till present date, even though generation started much earlier in neighbouring basins (Brownfield & Charpentier 2006). The repeated occurrence of mass-transport deposits in the area suggests an unstable slope throughout the Cenozoic. Understanding their distribution as well as those of the fluid flow features is very critical to exploration and production as they would form potential geohazards for offshore facilities installations and subsequent drilling (Posamentier & Martinsen 2011).

Mass-transport deposits (MTDs), deep-water channels, and sediment waves form important components of the continental slope of the Nigeria Transform Margin. MTDs are common in deep-water settings and easily recognised on seismic sections due to their chaotic internal character, extensive nature and distinctive external geometry (Shipp *et al.,* 2011). Integration of 2D/3D seismic data, side-scan sonar, multibeam bathymetry, well data and outcrop studies have improved understanding of MTDs in the last few decades; leading to better knowledge on their geometries, distribution, evolution and relationship with other depositional elements (Nissen *et al.,* 1999; Posamentier & Kolla 2003; Moscardelli *et al.,* 2006; Shipp *et al.,* 2011). The MTDs form up to 20 % of the entire succession with high-level of preservation of its main components such as head scarps, lateral margins, deformed blocks and ramps. These components were used as kinematic indicators to unravel the evolution and direction of translation of failed sediments (Bull *et al,* 2009). The association of MTDs with turbidites, which constitute significant target for deep-water drilling, suggests the need to map their lateral and vertical distribution and to understand their morphology (Shipp *et al.,* 2011; Nelson *et al.,* 2011).

The aim of this paper is to document the occurrence of MTDs and other depositional elements and fluid flow features along the Nigeria Transform Margin. This includes details of their spatial distribution, mode of occurrence as well as their usefulness in understanding the evolution and fluid flow of the basin. Main results from the analysis of 3D seismic data include; (1) sub-division of the post-transform section into five (5) main seismic units separated by major unconformities and surfaces; (2) spatial and temporal distribution of mass transport deposits through time; (3) documentation of fluid-flow features which includes pockmarks, pipes, furrows, bottom-simulating reflectors (BSRs) restricted in the eastern part of the area and their relationship with structural highs, deep-water channels and regional faults; and (4) the first documentation of polygonal faults along the Nigeria Transform Margin. The stratigraphic framework and features mentioned above show the transition between a giant-delta dominated eastern section and the more sediment starved steeper margin in the west, which is unique to this part of offshore Nigeria.

The study area is of major interest due to the hydrocarbon exploration potentials realised from the Aje field and Ogo discovery, making this study relevant to exploration. Hydrocarbon generation within the basin began in the Late Miocene and continues till present date, even though generation started much earlier in neighbouring basins (Brownfield & Charpentier 2006). The repeated occurrence of mass-transport deposits in the area suggests an unstable slope throughout the Cenozoic. Understanding their distribution as well as those of the fluid flow features is very critical to exploration and production as they would form potential geohazards for offshore facilities installations and subsequent drilling (Posamentier & Martinsen 2011).

2 GEOLOGICAL SETTING

The study area (Fig. 1) is located within the Dahomey-Benin basin, which stretches from southeastern Ghana to southwestern Nigeria (Obaje 2009). The basin is separated from the Niger Delta by the Okitipupa ridge (Obaje 2009). This basin forms part of the east-west aligned basins within the Gulf of Guinea. These basins were initiated during the Late Jurassic rifting between the African and South American plates; and are characterised by transform and wrench faults formed during the separation that resulted in similarities between the structural and stratigraphic elements within these basins (Greenhalgh *et al.,* 2011). The Nigerian Transform Margin (study area) and the other basins in the Gulf of Guinea contrast other regional passive-margin basins, such as the Lower Congo and Angola basins, by the influence of transform tectonics and the absence of salt tectonics (MacGregor *et al.,* 2003).

Basin evolution spanned three phases separated by major unconformities (Fig. 2). These include pre-transform or pre-rift (Late Proterozoic to Late Jurassic; not shown in the stratigraphic column), syn-transform or syn-rift (Late Jurassic to Early Cretaceous) and post-transform or post-rift (Late Cretaceous to Holocene) (Brownfield & Charpentier 2006). The Gulf of Guinea formed at the end of Late Jurassic to Early Cretaceous and was characterised by transform and block faulting above a regionally extensive Paleozoic basin during the breakup of the north Atlantic (separation of North America from Europe and Africa) that started during the Late Permian to Early Triassic (Ziegler 1988). Breakup of the African and South American continental crust began in the Early Albian and formed basins separated by transform faults (Blarez & Mascle 1988). The culmination of transform tectonism in the middle to Late Albian coincided with initial breakup of oceanic crust along the continents and formed the Gulf of Guinea initially as an anoxic oceanic basin; but by the beginning of Campanian, the Gulf of Guinea and the rest of the Atlantic Ocean had become an open-marine seaway (Brownfield & Charpentier 2006).

For this study, we summarize the post-transform succession, which the studied interval encompasses (Fig. 2). The Top Albian unconformity marked the end of the syn-transform phase, this was followed by thermal subsidence that continued till present day (Greenhalgh *et al.,* 2011). In the middle to Late Cretaceous, deeply incised canyons were eroded into the shelf during relative sea-level falls and transported sediments into the basin as large turbidite fans, which are the main reservoir targets along the transform margin (Fig. 2) (Brownfield & Charpentier 2006; Greenhalgh *et al.,* 2011). These sandstones were deposited within the Araromi and Agwu Shale Formation, which may have formed source rocks and seals for the reservoirs (Fig. 2) (Borsato *et al.,* 2012).

Non-marine to marginal marine conditions prevailed during the middle Cretaceous and are expected to contain gas-prone source rocks (MacGregor 2003; Brownfield & Charpentier 2006). Sediments deposited

during the Late Cretaceous in the basin are divided into two main stratigraphic units; the Abeokuta and Araromi Formations (Obaje 2009). Sandstone of the Araromi Formations forms the reservoir sands of the Aje and Seme fields in Nigeria and Benin, respectively (Fig. 2). Tertiary rocks unconformably overlie Cretaceous rocks and comprise Paleocene to Eocene marine shales of the Imo Shale Formation and interbedded with Ameki Formation sandstones in the study area (Fig. 2). A major Oligocene-Miocene unconformity separated the Early Tertiary succession from Miocene marine rocks (Fig. 2) (Brownfield & Charpentier 2006; Borsato *et al.,* 2012). Generation and migration of hydrocarbon within the Dahomey-Benin basin started during the Miocene and continued till present-day (MacGregor 2003; Brownfield & Charpentier 2006). Associated fluid flow features are concentrated within Pliocene to recent sediments.

3 DATASET AND METHODS

Dataset

The study area is located offshore the western part of Nigeria within the West Africa Transform Margin covering Petroleum Prospecting License 302, 301 and 300 (PPL) (Fig. 1b). It is bounded to the north by Aje field and Ogo discovery within OML 113 and OPL 310 respectively, to the west by the Hihon and Fifa fields and to the east by the Niger-Delta basin (Fig. 1a).

A 2,845 km^2 of GeoStreamer, 3D high-resolution seismic data from the West African Transform Margin was provided by Petroleum Geo-services (PGS). The GeoStreamer data provides clearer, more accurate and reliable dataset, with better resolution for the interpretation than traditional seismic data (Tab. 1. The 3D seismic data are pre-stack time migrated with a bin size (inline and crossline spacing) of 12.5 m x 12.5 m. In most parts of the area, reflector continuity suggests good data quality except in the interval below a channel complex in the eastern part of the study area. The seismic data are zero- phase processed with normal SEG polarity, such that an increase in acoustic impedance (hard reflections) is represented by positive amplitude (red peaks). This was determined from a phase analysis of the seabed. Frequency, horizontal and vertical resolutions were calculated for each unit assuming an average seismic velocity (*V)* of 2000 m/s (Tab. 1). Thickness conversion used the same p-wave velocity. Unfortunately, no well data were available for the study making it difficult to ascertain actual lithology. Horizon and sequence ages were determined based on the nearby Aje Field (Appen).

Methods

The study area was divided into two areas for ease of description: Area 1 - the eastern part, which is characterised mainly by the presence of fluid flow features (fluid flow zone) and Area 2, which is dominated by irregular and deformed seismic geometries (mass-transport deposit zone). Each of the areas represents approximately the limits of these features (Fig. 3). Six major horizons were mapped using 2D and 3D tracking using Schlumberger Petrel. These horizons were correlated with horizons in the survey north of the study area in OML133 (Aje field), therefore, ages of horizons are based on previous interpretation (Fig. 2). Seismic stratigraphic techniques based on seismic facies, reflection continuity and terminations were applied to establish the seismic stratigraphic framework of the area (Mitchum *et al.,* 1977; Catuneanu, *2022*).

Several horizons between the main horizons were produced using Paleoscan; an automated, seismic interpretation software. Time surface maps were generated from the horizons and used to create two-way-time (TWT) thickness and attribute maps (variance, root mean square (RMS), maximum amplitude, dip angle and dip azimuth). The attributes support the of features like MTDs, channels, faults, pockmarks, and furrows observed in the area. Time slices were used for detecting polygonal faults. Iso-proportional slices were also generated from spectral frequency decomposition in SVI Pro to produce Red-Green-Blue (RGB) colour blends to image and analyse deep-water channels in a consistent manner in Area 1 of the study. Local high amplitude seismic anomalies manifested on the seismic (i.e., bright spots) were identified to indicate possible gas accumulation.

4 OBSERVATIONS AND RESULTS

This section is structured into 2 parts, the first part will present observations and results of the stratigraphic units and depositional elements, while the second part will cover fluid flow features. We observe four distinct and dominant deep-water depositional elements: (i) MTDs, (ii) channels, (iii) sediment waves, and (iv) hemipelagic/background deposits, and five fluid-flow features: (i) pipes, (ii) pockmarks, (iii) bottom simulating reflector (BSR), (iv) seabed mound and (iv) polygonal faults.

(i) Sequence stratigraphic units and seabed morphology

The studied interval encompasses the entire Cenozoic and Cretaceous successions bounded by the Late Albian unconformity at the base and the present-day seabed at the top. The entire Cretaceous and Cenozoic successions represent the post-transform interval (Figs. 2 & 4). 3D seismic interpretation indicates presence of an up to 2 s TWT (2 km) thick post-transform interval (Fig. 4). The tectono-stratigraphic framework of the interval is controlled by transform faulting that terminated in the Late Albian. This was followed by deposition of thick post-transform sediments above the Top Albian unconformity (MacGregor *et al.,* 2003). The unconformity is represented by a strong positive amplitude reflection mapped only in the northern part due to date coverage. The post-transform interval was divided into five (5) seismic units bounded by six (6) surfaces. Units are described in this work as SU1 to SU5, from oldest to youngest (Figs. 4 & 5).

SU1 comprises the Cretaceous sequence bounded at the top and base by the Cretaceous and Albian unconformities, respectively (Fig. 2). The unit is characterised by relatively low amplitude reflections (Fig. 4). Although no well data are available to determine lithology, previous studies confirmed the unit is dominated by sandstone and shale (Brownfield & Charpentier 2006). The Late Cretaceous-aged sandstones form the reservoirs for the Aje and Seme fields and equivalent of the Jubilee field in Ghana (Borsato *et al.*, 2012) (Fig. 2). Unit thickness reaches up to 800 ms TWT in the west but is absent where the top Cretaceous unconformity merges with the top Albian unconformity at ~3500 ms TWT (Fig. 5a).

SU2 is bounded at the top by a major unconformity (Eocene-Oligocene?) and at the base by the top Cretaceous unconformity. This unit is characterised by low to high amplitudes and continuous reflections that sometimes undulate, especially in the centre part of the study area (Fig. 4b). Two-way-time thickness map shows sediment thickness within the unit reaches up to 1100 ms TWT comprising of the Eocene sequence (Fig. 5b).

SU2 is overlain by SU3. This unit is bounded at the top by the Oligocene-Miocene unconformity and at the base by the Eocene-Oligocene unconformity (Figs. 2 & 4). The lower surface erodes into the underlying unit (Fig. 4a). Internally, the unit is characterised by low to moderate amplitude reflections. Chaotic reflections are also prominent within the unit. The TWT thickness map reveals a series of north-south oriented, elongated anticlines separated by alternating lows (Figs. 4b & 5c). Thickness reaches up to 700 ms TWT in the western part and up to 350 ms TWT where the anticlines are present.

SU4 is characterised by very low amplitude but parallel reflections that is bounded at the base by the Oligocene-Miocene unconformity. The unit top was placed at the change in seismic facies from underlying low-amplitude, transparent reflections to overlying low to high-amplitude reflections belonging to SU5 (Fig. 4). SU4 is relatively thin in the centre of the study area, with thickness only about 200 ms TWT (Fig. 5d).

SU5 represents the youngest unit described in the study. The unit is bounded at the top and base by the seabed and the top of the Miocene section, respectively. It is characterised by low to high-amplitude reflections that are often chaotic (Fig. 4). Thickness within the unit reaches up to 1100 ms TWT where channels are observed. The SU5 forms a unique part in the study due to the local presence of depositional and fluid flow features within the unit that provides understanding of the basin evolution and petroleum system (Fig. 2). The overall structural framework of the basin is dominated by north-south elongated anticlines and northwest-southeast regional normal faults that are clearly imaged in the seismic data.

The morphology of the seabed in the study area is imaged in detail by structure and attribute maps (Figs. 6 & 7). Dip angle and variance attribute on the seabed surface highlights key features and provides an overview of related shallow subsurface features in both areas 1 and 2. Area 1 of the seabed is mainly characterised by seabed depressions, while Area 2 shows is dominated by irregular geometries with localised structural highs and blocks towards the middle (Fig. 6). These blocks are protruding, forming a positive topography on the seabed.

(i) Mass Transport Deposits (MTDs)

Low-amplitude, transparent and chaotic facies are prominent in the study area. They form deformed units and blocks as high as 350 ms TWT and ~ 2 to 10 km in length (Fig. 7) and make up ~20 % of the succession. Similar features in seismic are well represented from outcrop and core data across the globe, ranging from few metres to hundreds of kilometres in length, often on the slope and basin-floor in deep-water settings (Posamentier & Martinsen 2011). Several authors have interpreted these as mass-transport deposits (MTDs) that form when shear stress oriented down the slope overcomes shear strength of a weaker layer in the slope succession, such that large volume of sediments is mobilisedby slope failure (Zhu et al., 2011). MTDs are easily recognised on seismic sections due to their chaotic internal character, large size, extensive nature and distinctive external geometry (Shipps et al., 2011), all of which are similar to here (Fig. 7).

The morphology of MTDs is often grouped under three main domains: headwall, translational and toe, each of which can provide information on the direction of failure and evolution of the MTD (Bull et al., 2009). The headwall consists of the upslope region dominated mainly by extensional processes that form the headwall scarps, extensional ridges, and blocks (Bull *et al.,* 2009). The headwall scarp exhibits an actuate geometry and provides information on direction of movement of the sediments. In our case, sediments moved from northeast to southwest (Fig. 8). The translational domain, which forms the main body of the MTDs is grouped under lateral margins (scarps; strike slip deformation), basal shear surface (ramps and flats; grooves and striations), internal body of MTD (translated and outrunner blocks; slump folds) and top slide surface (longitudinal shears; secondary flow fabrics). Lateral margins are easily

identified on seabed MTDs (Figs. 7a, 8). Lateral scarps/margins form the sides of the MTDs and are generally parallel to slope direction processes (Bull *et al.,* 2009). Deformed blocks as high as 350 ms TWT and ~ 2 km in length are observed within SU 3 and 4 (Fig. 9). They are similar in height to rafted blocks observed in Hinlopen Slide on the northern Svalbard Margin in the Arctic Ocean which are as high as 450 m and more than 5 km wide (Vanneste *et al.,* 2006). Reflections within the blocks, if preserved, are sometimes rotated to near vertical and often appear chaotic.

The toe domain represents the downslope part of a mass-transport deposit, where the MTD terminates or the region at which the movement stopped (Martinez *et al.,* 2005; Bull *et al.,* 2009). It is made up of compressional structures such as thrusts, folds, and pressure ridges (Figs. 7, 9b). Pressure ridges are the curvi-linear surface expressions of incipient thrusting at the distal end of a mass movement deposit.

Utilising a combination of time surface maps and attribute extraction on the basal surfaces helped to investigate the presence and distribution of mass-transport deposits. Based on this, we have mapped large-scale MTDs from seismic units 2 to 5 (Fig. 10). Figure 10 highlights the MTDs outline produced from mapping of the basal surface of each MTD. In total, 22 mass-transport deposits were mapped, ranging from a few kilometres to tens of kilometres in length and between 50 to 450 ms TWT in thickness. Individual volumes are not calculated but areal extent of the mass-transport deposits gives an idea of the volumes of failed sediments along the slope during the Cenozoic.

(ii) Deep-water channels

We observe distinct seismic characteristics, such as high- to medium-amplitude reflections that are stacked within V- and U-shaped structures in cross sections and form meander shapes in plan-view (Figs. 3, 6, 8, 11). Single V- or U-shaped structure are ~5 km wide and 50 ms TWT thick; when stacked up, they are up to 400 ms TWT in thickness (Fig. 11). Iso-proportional slices through the RGB frequency decomposition colour blend volume show meandering trends from northeast to southwest for ~20 km in the eastern part of the area (Figs. 6, 11). The margin of this meandering feature is clearly distinguished from the blended volume and well imaged on the seabed. Similar geometries have been observed and interpreted as deep-water channel systems. Based on similar characteristics observed here, we interpret these features as deep-water channel complex systems. These channels form along an important component of continental slopes on the eastern Nigeria Transform Margin (Figs. 11 & 12) and include active and buried channels. Channel complexes are often described by their sinuosity (Posamentier and Kolla, 2003) and we observed both highly sinuous and linear channels.

The main channel complex presented in this paper is highly sinuous and consists of stacks of buried (CC2 – CC4) and active channels (CC1 and CC5) with strongly incised bases, as imaged from iso-proportional slices taken from the seabed (t10) to the base of the high-amplitude, reflection package (t1) (Fig. 11). The full length of the channel system cannot be determined due to data extent (Fig. 3). Mapping of the channels in Area 1 was important as they form part of the fluid flow history in the area. Circular depressions are observed along channel margins and within channel axis of the channel complexes. Lithology within the channels cannot be ascertained without well data but based on high-amplitude character; channels are likely to be sandstone-rich. Analysis of the iso-proportional slices provides insights to the channel complex evolution with time, with each slice represented here as a Time i.e t1 to t10 (Fig. 11). CC1 becomes more confined with time (time 10). CC5 is less sinuous and looks more like a levee of another channel but its location at the end of the survey makes it challenging to confirm this (Fig. 6).

Figure 12 shows continuous incisions, 10 – 15 m deep and up to 250 m wide on the seabed in Area 2. These form linear and narrow features in seismic profiles and on TWT maps. They are interpreted as linear

channels like those observed offshore Angola formed from erosional lineation on the slope created by large and infrequent turbidity current (Gee & Gawthorpe, 2007).

(iii) Sediment waves

Seismic attribute extraction at -50 ms below the seabed reveals a 25 km long curvi-linear feature in the eastern part of the study area, close to the channel complex (Fig. 13a). Average width is 2 km, which increases abruptly in the southern part and forms a lobe similar to terminal lobes in deep-water environments. It has the same northeast-southwest orientation as the main channel system but terminates before the end of the survey. In seismic cross-sections, the linear feature is manifested as bright amplitude lateral anomalies with a normal phase polarity, which is also highlighted on RMS amplitude extractions (Fig. 13). A seismic profile through the lobate part of the feature shows the anomalies are constrained within what resembles a cut-off loop of the channel and interpreted as an upslope-migrating sediment-wave train (Fig. 13c).

The sediment waves developed within what could have been an abandoned channel, hence it mimics the shape of a channel (Fig. 13a). We assume the sediment waves were formed by turbidity currents. Sediment waves originating from turbidity currents and located within leveed channel complexes and channel over bank deposits have been observed in the Niger Delta basin (Posamentier & Kolla 2003; Sutton & Mitchum, 2011). The location of the sediment waves observed here, some 100 km westward of the shelf-slope break and some 1.5-2 km below sea level highlights the distributive power of gravity-driven currents.

(iv) Fluid Flow Phenomena

(a) Pipes and high-amplitude reflections

Vertical and narrow columns are clearly visible from seismic cross section in the upper stratigraphy of seismic unit SU5 in the eastern study area (Area 1). They are between 50-80 m wide and extend about 400 ms below the seabed (Figs. 14a, b). Within the features, seismic response is slightly distorted, and reflections are characterised by subtle, positive relief geometry (Figs. 14c-g) but surrounding reflections appear continuous. These narrow columns are often located below seabed depressions and have a circular to oval shape on time slice (inset of Fig. 14a). In the northern part of Area 1, these vertical columns terminate downwards above a structural high at about 2150 ms TWT below the present-day seabed. Similar features have been interpreted as blow-out pipes formed from fluid migration through the stratigraphic succession (Løseth *et al.,* 2001; 2011; Gay *et al.,* 2007; Cartwright *et al.,* 2007; Moss & Cartwright 2010; Huuse *et al.,* 2010).

In the study area, the structural high is faulted at the crest by series of normal faults (Fig. 14a). The quality of the amplitude reflections diminishes within the vertical columns but increases towards the top of the structural high. This is seen clearly on Figs 14d and 14f. Positive, high amplitude anomalies are often observed either directly below the column (Fig. 14d) or adjacent to it at the level at which the columns terminate (Fig. 14a & f). The seabed has a normal polarity, such that the negative continuous reflection (blue) is overlayed by a very strong positive continuous reflection, which is the seabed (red) (inset image in Fig. 14a). In most cases, the high-amplitude reflections associated with these pipes have a reversed polarity to the seabed, such that the red, strong positive reflection is overlayed by the blue negative reflection (Fig. 14a, d & f) (Schroot & Schuttenhelm, 2003; Andreassen *et al.,* 2007). These amplitude anomalies form bright spots and could be associated with gas accumulation. Occasionally, these bright spots terminate against the fault plane (Fig. 14f). Similar amplitude patterns have been described in other parts of the deep-water Niger Delta basin (Loseth *et al.,* 2001; 2011) and Barents Sea (Andreassen *et al.,*

2007) and are often interpreted as gas charged sands within deep-marine reservoir channels or fans. Based on the observations presented here, the vertical columns are interpreted as pipes. These pipes can act as fluid migration pathways to the palaeo- or present-day seabed (Gay *et al.,* 2004; Ligtenberg 2005; Loseth *et al.,* 2009; Ho *et al.,* 2012).

(b) Pockmarks

Numerous depressions ranging from 60 to 480 m wide are identified on the seabed from seismic cross-sections (Figs. 14, 15 & 16). They exhibit circular, oval, or elongated geometries in plan-view and are randomly distributed (Fig. 14b). These depressions have been observed both on the present-day seabed and palaeo-seabed. Different types of depressions are described below based on their geometry, location, and occurrence with other depositional elements in the area.

Isolated/scattered and pipe-related pockmarks

In seismic cross-sections, V or U-shaped depressions are observed on the present-day seabed on the northern part of Area 1. These depressions are up to 15 ms TWT deep and 60 m wide. Some occur as single, isolated depressions and others are observed scattered randomly on the seabed above a structural high (Fig. 14). Spacing between individual pockmarks is irregular and they occur directly above underlying vertical columns interpreted in the previous section as pipes (Fig. 14a). The location of these isolated pockmarks above vertical pipes could be suggested that they are genetically related. The relationship between pockmarks, pipes and sandstone reservoirs was identified in the deep-water Niger Delta by Loseth *et al. (*2001; 2011), who suggested that seabed craters formed from gas expulsion from an underlying hydrocarbon-charged reservoir and through 1 km of overburden.

Stacked pockmarks

Five horizons were interpreted locally around what appears to be vertically stacked depressions between 1975-2275 ms TWT in the eastern part of the study area (Fig. 15a). In plan-view, depressions exhibit circular geometry on each of the horizons (Fig. 15b). The depth of individual depression is between 10-35 ms TWT and width varies from 270-480 m from shoulder to shoulder (Fig. 15b). The depth and width of the stacked pockmarks increase with stratigraphic depth (Figs. 15bi-iv). This relationship changes on the last horizon mapped (Fig. 15bv). It is unclear what is controlling the change in dimensions, but we observe the deepest depression coincides with an increase in amplitude (Fig. 15a). The stacked depressions are associated with the hanging wall of faults and high-amplitude, soft-kick reflections (possible gas accumulation) that terminate against the fault plane (Fig. 15a & d). They are interpreted as stacked pockmarks like those from the Lower Congo Basin and are indicative of repeated fluid expulsion within the sedimentary column (Cartwright *et al.,* 2007; Andresen & Huuse 2008; Martinez *et al.,* 2011).

Fault-related pockmarks

Circular or elongated depressions are observed either along the hanging wall of faults (Fig. 15d) or directly above normal fault planes (Fig. 15e) like those observed in other parts of the West African margin (Pilcher & Argent, 2007). These are clearly imaged on seismic profiles and attribute maps below the seabed (Figs. 15d-15f). The faults are oriented northwest-southeast and occasionally offset the present-day seabed creating linear depressions on the seabed, suggesting the faults are likely to be still active (Fig. 15f). The circular or elongated depressions observed on the Nigeria Transform Margin are interpreted as pockmarks (Hovland & Judd, 1988) and likely indicate fluid leakage through faults (Ligtenberg, 2005).

Channel-related pockmarks

The variance attribute extracted on the seabed shows many depressions (red arrows on Fig. 16b) above and along margins of active and buried channel complexes. These depressions are ~ 200-300 m wide and ~50 ms TWT deep below the seabed. They are mostly circular in plan-view and more regularly spaced (~1 km) than those observed above the structural high (Fig. 14b). Based on their characteristics, they are interpreted as pockmarks (Fig. 16) (Hovland & Judd 1988). The pockmarks follow the meandering geometry of the buried channels described above (Fig. 15). Lithology within the channels have been interpreted as sandstone based on their high-amplitude seismic expressions. Presence of pockmarks above stacked turbiditic palaeo-channels have been well-documented in the Lower Congo basin (Gay *et al.,* 2003, 2004, 2006, 2007) and have been attributed to fluid expulsion from active and buried channels with the fluids sourced directly from deeper intervals (Gay *et al.,* 2006, 2007). A series of small faults are observed above the buried channels, and these may have facilitated upward fluid migration from underlying buried channels, forming pockmarks on the present-day seabed (Fig. 16a). Fluid expulsion from deep-water channels has also been associated with emplacement of sandstone injectite in the deep-water Niger delta towards the eastern part of the study area (Davies, 2003).

Elongated pockmarks

A series of high-amplitude, wedge-shaped anomalies in cross-sections are observed at ~ 25 ms TWT below the seabed (Fig. 17). These anomalies are characterised by two full reflection cycles starting with a hard-kick at the top and a soft-kick at the bottom. They are isolated packages, about 25 ms TWT thick and terminate against fault planes (Fig. 17b). The thickness of each reflection package increases towards the fault plane and wedges away from it. Amplitude diminishes away from the fault plane into continuous reflections like the surrounding strata (Figs. 17a, b & d). The high-amplitude packages are layer-bound and extend laterally for about 15 km. RMS attribute extracted on the yellow horizon (Fig. 17d) located ~100ms below the seabed, with a window length of 75 ms, revealed the plan-view geometry and distribution of these features as randomly spaced, circular-oval or elongated shaped depressions oriented in northwest-southeast or west-east direction (Fig. 17). Based on their geometries and similarities with previous interpretations of depressions in the area, they are also interpreted as pockmarks. These elongated pockmarks are up to 1500 m long and 200 m wide (Fig. 17d). Similar elongate depressions have been interpreted as furrows along the mid-Norwegian margin (Reiche *et al.,* 2011) and Lower Congo basin (Gay *et al.,* 2004); and attributed to volumetric contraction of sediments during early stages of compaction. They are linked to normal faults and could constitute bypass systems for upward movement of fluids.

We observe a unique relation between the underlying normal faults and the elongated pockmarks that is not clearly observed with the circular pockmarks (Fig. 17). Where underlying regional faults propagate through shallower sediments and wedge-shaped anomalies terminate against the fault plane, elongated pockmarks are formed (numbered 7-10 in Fig. 17).

This relationship could suggest a transition from individual circular to elongated pockmarks created from modification of the pockmark geometry by the faults (inset in Fig. 17d),. A similar transition model from circular pockmarks to elongated pockmarks (furrows) was proposed in the central North Sea and modification was attributed to movement of bottom currents (Kilhams *et al.,* 2011; Kalucke *et al..,* 2018). Since the first recognition of pockmarks on the Scotian shelf from sidescan records by King & MacLean (1970), these features have been documented in several basins in the world (Rise *et al.,* 1999; Ligtenberg 2005; Judd & Hovland 2007; Gay *et al.,* 2007; Andresen, 2012; Reiche *et al.,* 2011; Ostanin *et al.,* 2012).

(c) Gas-Hydrate Bottom Simulating Reflector (BSR)

The seismic cross section shows the presence of a continuous reflection with negative polarity (opposite amplitude relative to the seabed reflection) at about 300 ms below the seabed within SU5 (Fig. 18). The reflection tracks the seabed reflection but exhibits a cross-cutting relationship with surrounding stratigraphic reflections (Fig. 18c). The reflection is consistently located at the same depth below the present-day seabed (Fig. 18a). Below the reflection, high-amplitude packages with reverse polarity ('soft' events) are interpreted as free gas accumulations. A relationship is observed between this continuous reflection and the faults in this area such that the limit of the reflection can only be mapped in the area where the regional faults are present (Fig. 18c). Some of the faults terminate below the continuous reflection while others extend above it into the shallower section (Fig. 18a & b). We observed pockmarks on the present-day seabed above this reflection (Fig. 18e & d).

Based on geometry, reflection character, depth below the seabed, localised presence, and location of possible gas in the underlying interval, the reflection is interpreted as a bottom-simulating reflector (BSR) (cf. Shipley *et al.,* 1979). The negative acoustic response is formed from the contrast between overlying high-velocity gas hydrate and the underlying low-velocity, free gas-saturated sediments (Gay *et al.,* 2003; Berndt *et al.,* 2004). Gas hydrate BSRs are associated with hydrate stability and often observed in deep-water settings (Shipley *et al.,* 1979; Gay *et al.,* 2007; Serie *et al.,* 2012). Gas hydrates have previously been observed using seismic data on the continental slope offshore Nigeria to southern Angola (Cunningham & Lindholm, 2000), which supports our interpretation of gas-hydrate related BSR in this study.

A basic consideration of depth and temperature conditions for the BSR allows a first-pass estimation of BSR temperature and heat flow according to data presented by Grevemeyer & Villinger (2001). The seabed depth is approximately 1.8 km and the BSR depth about 300 ms below that, corresponding to a total depth of 2040-2100 m below sea level (assuming water velocity of 1.5 km/s and sediment velocities between 1.6-2.0 km/s). Plotting this on the gas hydrate stability curve for hydrostatic pressure and sea-water salinity, allows the estimation of BSR temperature: 17-18 °C. Assuming the seabed temperature is 3-4 °C, this would give a thermal gradient in the hydrate stability zone of about 50-60 °C/100m. Assuming a thermal conductivity close to 1 W/m/K, this would suggest a heat flow for the BSR location of 50-60 mW/m^2, based on parameters provided by Grevemeyer & Villinger (2001).

Previously, presence of gas hydrates and BSR were thought to impede upward flow of fluid through the gas hydrate stability zone, but frequent identification of fluid flow phenomena such as pockmarks, pipes, and gas hydrate pingoes above BSRs suggests hydrates may act as a baffle rather than a barrier to fluid flow (Cummingham & Lindolm 2000; Hovland 2005; Gay *et al.,* 2006a; Ostanin *et al.,* 2012; Serie *et al.,* 2012). The interval above the BSR here contains small extensional faults and that could have permitted migration of gas through the sedimentary column to the seabed. Hydrate dissolution has been proposed as an alternative mechanism for pockmark formation in the Niger Delta due to excessive overpressure generated during dissolution process (Sultan *et al.,* 2010).

(d) Seabed Mound

In the south-eastern part of the study of Area 1, a feature with positive topography set within a flanking moat is observed on the seabed. It is well-imaged from the time-structure, attribute, and frequency decomposition maps of the seabed as an isolated, mounded structure (Fig. 19) that is ~30 ms TWT in thickness and 500 m wide. At about 20 ms below the top of the feature, there is a marked increase in amplitude strength (Figs. 19b & c). Below the high-amplitude zone is a cylindrical zone of convex-upward

dim reflections~ 300 ms TWT in vertical extent between 2425 and 2725 ms. We interpret the convex-upward reflections as a series of stacked pull-up geometries deflected about 20 ms TWT upward relative to the reflections in the surrounding area.

The pull up can be used to provide a first order estimate of interval velocity for the mound, provided the mound TWT thickness is known and based on an assumption of the background velocity. The imaging provides some constraints, and we estimate the mound TWT-thickness to be around 30 ms TWT. Based on a pull-up of 20 ms TWT and a background velocity of 2 km/s, some combinations of mound velocity and thickness can be estimated. For a realistic maximum velocity of 4 km/s (close to massive hydrate or porous limestone) would imply a mound thickness of 40 m, while a lower velocity of 3.3 km/s would suggest a mound thickness of 50 m. Although surrounding reflections can be traced within the vertical column, reflections strength is weak and discontinuous. The transition between the surrounding reflections and vertical column is abrupt and clearly imaged in cross section (Fig. 19b).
Time slices through the vertical column below the mound show circular geometry of the column and a neighboring pockmark, which is located about 5 km from the main channel complex (Figs. 19e. The vertical column is rooted within high-amplitude, semi-continuous to discontinuous reflection packages interpreted as a sandstone-rich channel complex (Fig. 19b & c). Opacity rendering was applied on a cropped volume to show relationship between the mound, vertical column, and underlying sandstone-rich channels (Fig. 19d).

The possible origin for this seabed mound was investigated based on similar dome-shaped or circular features on the seabed elsewhere. These include mud volcano, shale diapir, salt body, carbonate mound, (Stewart 1999) or a hydrate pingo (Serie *et al.,* 2012). No well or core information is available in the study area to determine lithology, but a salt origin can be discarded through a lack halokinesis in the area. Gay *et al.,* (2007) described a similar feature from Lower Congo Basin and core analysis suggests cold-water corals interbedded with hemipelagic muds. Similar palaeo-seabed mounds observed on the mid-Miocene unconformity in the Norwegian-Danish basin and Northern North Sea were interpreted as sand extrudite (Andresen e*t al.,* 2009; Olobayo *et al.,* 2015b). Seismic amplitude character below the mound is similar to those described from the Angola Margin as gas hydrate pingoes (Serie *et al.,* 2012). Mound volcanoes formed from periodic expulsions of gases, liquids and sediments to the seabed have been described from the western slope of the Niger-Delta basin, but the location of the mound above a possible sandstone-rich channel makes a hydrate mound unlikely (Graue 2000). However, due to the high velocity within the mound (~4 km/s) a sandstone origin is unlikely. Lithologies known to produce such high seismic velocities are often carbonates (Anselmetti & Eberli, 2012). We, therefore, propose a methane-derived, carbonate mound origin formed from fluid sourced from underlying channel sands (Figs. 16d & e) (Cauquil & Adamy 2008).

(e) Polygonal Faults

The seismic data reveal networks of small, extensional normal faults in the area (Fig. 20). These faults are well imaged in the first 400 ms TWT below the seabed (Figs. 20a & c). Fault throws are less than 12 m (between 3 – 11 m, 6 m average) and dip angle range of 41-50 ° (46 ° average) assuming a 2000 m/s velocity (Tab. 2). Time-structure map, original amplitude, and variance attribute extractions on horizons through the highly faulted succession shows faults form polygonal geometry in plan-view (Figs. 20 b & d). Based on observations above, we interpret these faults as polygonal faults, and this study presents the first documentation of such features in the Nigerian deep-water setting.

Similar faults have been interpreted as polygonal faults, which was first observed within the smectite-rich Eocene succession of the North Sea basin and defined as layer-bound faults formed from dewatering of fine-grained sediments, particularly mudstones, during early burial (Cartwright 1994; Lonergan & Cartwright, 1999; Lonergan *et al.,* 1998; Goulty 2001; Stuevold *et al*., 2003). They have since then been documented in many basins. These polygonal faults have similar dip angles to those recorded in the North Sea, but smaller fault throws (Tab. 2). They deform the SU3-SU5 and occur in two tiers separated by a non-polygonally faulted interval; the upper tier top terminates about 50 ms TWT below the seabed and is better-imaged than the lower tier in SU3. The polygonal faults are randomly oriented in most parts of the study area, but close to regional faults they do become linear and preferentially aligned with the NE-SW regional faults but perpendicular to the NW-SE regional faults (Fig. 20b & d).

In the Lower Congo basin, similar faults are documented within Pliocene-aged sediments below the seabed and have similar throws as those observed along the Nigeria Transform Margin (Tab. 2). Another characteristic feature observed between the faults along both margins is occurrence of alternating layers with low and high amplitude anomalies through the faulted interval (Gay *et al.,* 2004). Where this is observed in the study area, the polygonal faults are more visible in seismic cross sections, and this could be related to lithological characteristics.

1
2

5 DISCUSSION

This section summarises the mechanism of MTD formation, controls on fluid flow distribution and fluid sources. A summary diagram highlights all the deep-water depositional elements and fluid flow phenomena interpreted in the study area (Fig. 21).

Mechanism of MTD formation

Mass-transport deposits can be found at a variety of scales ranging from small-scale as in cores, medium-scale in outcrop and to regional seismic scales such as the Storegga slide offshore Norway (Bull *et al.,* 2009; Shipp *et al.,* 2011; Dykstra *et al.,* 2014). Regardless of the scale at which they occur, MTDs are a direct response to slope instability in sedimentary basins (Posamentier & Martinsen 2011). The MTDs observed here represent multiple events of slope mobilisation on the Nigeria Transform Margin and occur primarily in Area 2. We refer to this as the mass-transport deposit zone (Fig. 22a). They include both buried and active MTDs from SU2 to present day suggesting repeated slope failure throughout the Cenozoic (Fig. 10). These mass-transport deposits occur in association with other deep-water deposition elements such as channel complexes and sediment waves (Fig. 6).

We investigated the plausibility of different MTD triggering mechanisms in our study area and discuss them below. Silica diagenetic transformation has been proposed previously as a trigger for submarine failure in the Faroe-Shetland basin (Davies & Clark 2006). Elevated pore pressure from expulsion of pore fluids during conversion of opal A to CT can result in rapid compaction, which could reduce sediment shear strength, making it susceptible to failure. The opal A to CT transformation boundary is often manifested on seismic as a high-amplitude, hard-kick reflection (similar to the seabed) formed as a result of increased acoustic impedance (Davies & Cartwright, 2002). Diagenetic silica transformations are observed in seismic data further west along the West African Transform margin, but in the present study area we do not see evidence of an opal A to opal CT boundary. Therefore, this potential trigger mechanism is deemed unlikely in our study area.

The BSR is as the contact between gas hydrate bearing sediments and sediments hosting free gas within SU5 (Pliocene- recent) sediments in Area 1, which is also where fluid flow phenomena dominate. From the MTD maps, we observe that MTDs occur more extensively beyond the BSR where the hydrate stability zone would be thicker. However, it is difficult to establish a relationship between MTDs formed sometime in the past and the BSR's current location. An alternative and common mechanism for formation of episodic mass-transport deposit is sea-level change (Nelson *et al.,* 2011). We have no absolute ages for the MTDs in the area to be able to correlate with sea level changes, making it difficult to connect MTD sheets with eustasy. However, there was a significant global sea level fall at the onset of the Pliocene (MacGregor 2003; Brownfield & Charpentier 2006) and this correlates with the period showing a major increase in MTD development in our study area (Fig. 10).

The Nigeria Transform Margin falls within the Equatorial conjugate margin characterised by complex wrench and transform faulting. However, from previous studies, transform tectonism was only active until Middle to Late Albian (Brownfield & Charpentier 2006). The Late Albian unconformity represents the lower bounding surface of our entire study interval – we do not have data below this interval – and regional mapping of the unconformity shows that transform tectonism and faulting were no longer active at this time even crustal extension continued, causing increased clastic deposition and thermal subsidence that continued till the Tertiary (Brownfield & Charpentier 2006).

Net sediment accumulation rate from the Late Albian unconformity to present day was estimated using a simple calculation method using two-way-time thickness maps and a constant velocity of 2 km/s (cf. Jordt *et al.,* 2000) (Tab. 3) (Fig. 23). Results do not account for compaction, burial or erosion, but do suggest the magnitude of failed sediment increased through time in the area with an exception in SU4, but overall an obvious increase in sediment accumulation is observed (Figs. 10, 23, Table 3). This can also be observed from the distribution maps of the MTDs (Fig. 10). Based on this, we suggest that the formation of episodic MTDs on the Nigeria Transform Margin was mainly driven by high sedimentation and the increased frequency through time was also controlled by increased sedimentation. Sea-level change could have contributed to this, but we do not have evidence to support this claim apart from correlative global sea-level fall during the Pliocene when in SU5 was deposited in Area 2.

Over steepening of the slope could also be a contributing factor to slope failure in the area. Slope gradient measured is up to ~8° for the present day, as revealed from the dip angle map of the seabed in Fig. 6a, and this could have enhanced rapid deposition or slope progradation of sediments, especially in an area with high sedimentation rate (Zhu *et al.,* 2011).

Controls on fluid flow features and distribution

Interpretation and analysis of 3D seismic data presented in previous sections reveal detailed geometries and spatial distribution of numerous fluid flow features within SU5 in Area 1 of the Nigeria Transform Margin fluid flow (Figs. 14-22). This area is considered as the fluid flow zone. We rely on seismic interpretation in absence of geochemical data or surface seepage expressions to come to our conclusions. Analysis of these features was carried out using volume and surface attribute extractions to reveal their geometries and spatial distribution along the margin and identify features such as pockmarks, pipes, BSR, seabed mound and polygonal faults (Fig. 21). They occur both on the present-day and palaeo-seabed.

These fluid flow features are surface expressions of fluid venting from an underlying source, which could be either gas, liquid or both; giving indication of the presence of an active petroleum system; or it could

be of biogenic origin (Hovland & Judd 1988, Rise *et al.,* 1999; Cartwright 2007; Gay *et al.,* 2007; Judd & Hovland 2007; Huuse *et al.,* 2010).

Based on our observations, we suggest these features have served as migration pathways either through focused zones of weaknesses along underlying faults or diffused within permeable sediments within sandstone-rich channels (Ligtenberg 2005; Pilcher & Argent 2007; Gay *et al., 2006,* 2007). Active petroleum plays exist along the West Africa Transform Margin, which includes the syn-transform Aptian-Albian fields such as Hihon, Fifa, Tano and the younger, post-transform Upper Cretaceous fields such as Aje, Panthere, Belier, which are sourced from Cretaceous shales (Greenhalgh *et al.,* 2011). Most of the regional faults in Area 1 are deep-seated and reach the Cretaceous interval where source and reservoir rocks within the basin are located (Fig. 2). Pockmarks, pipes, and BSR interpreted in the area are related to the underlying regional faults (Figs. 22b, c, g-i) while the seabed mound and some pockmarks are related to active and buried channels (Figs. 22d-f). Seismic quality below the channels is poor and chaotic, which made it difficult to map regional faults below the channel complexes, if they exist (Fig. 4e). It is, therefore, assumed that fluids that generated pockmarks above the channels are likely to have been sourced from within the channels, but it is also possible they could have been sourced from deeper faults (Figs. 22e-i).

Fluid type, source and driving mechanism

A lack of geochemical data made it difficult to ascertain the type of fluid expelled during the formation of these fluid flow features. In the Lower Congo basin, core samples were taken from pockmarks for geochemical analysis, and this confirmed the presence of biogenic and thermogenic gas (Gay et al., 2006a). The presence of bright spots with reverse seabed polarity along fault planes and below pipes, and possible free gas below the BSR strongly suggests gas presence in the area (Figs. 14, 22b, d & g-i). The Aje field located in OML113 in the northern part of the study area is a successful gas field with its reservoirs within the Cretaceous interval (Figs. 1b, 2c). Recent drilling into Cretaceous sandstones in OPL310 (Ogo discovery) east of Aje field to the north of the study area also encountered significant accumulation of oil, supporting the notion of an active petroleum system in the area.

Based on this, we suggest that fluid type is likely to be either gas or oil. However, we cannot exclude that pore water expelled from reservoirs also contributed to it because of differential compaction of coarse-grained sediments and fine-grained mudstones. Regional faults, which are rooted within the Cretaceous interval, occur in association with fluid flow phenomena and are likely to have facilitated upward migration of fluid from deeper intervals. It is unclear whether the faults are sealing or not, but presence of fluid flow features or seal bypass systems in the shallow interval suggests leakage along faults (Cartwright *et al.,* 2007). We support both biogenic origin of hydrocarbon from shallow interval and thermogenic origin from deeper reservoirs or combination of both for hydrocarbon source in our study area. However, this cannot be confirmed without appropriate geochemical analysis (Judd & Hovland 2007).

In the study area, all the fluid flow features occur within the shallow Pliocene to recent section (SU5) (Fig. 22 b-i). This coincides with timing of hydrocarbon generation and migration in the Cretaceous source rocks within the Dahomey-Benin basin, which started in the late Miocene and continued till late, (Brownfield & Charpentier 2006). Based on this, we suggest timing of fluid flow products formation began after late Miocene till the present day and fluid flow could have been triggered because of hydrocarbon generation within the basin. This assumption favours a more thermogenic origin for the fluid formation in the area.

Implications

Our study has implications for hydrocarbon exploration and geohazards in the study area. The presence of MTDs and fluid-flow features are geological hazards as they result in slope instability and should be carefully investigated before placement of drilling infrastructures (Shipp *et al.,* 2011). MTDs constitute a significant portion of the succession in our study area and could impact sediment pathways and distribution. They can also serve as seals and reservoirs of source rock under the right conditions (Posamentier & Martinsen 2011).

Pockmarks, pipes and BSRs are evidence of shallow gas accumulation and expulsion, which can be due to a shallow biogenic gas system or the breach of deeper petroleum systems. Impacts of pockmarks and other seabed fluid flow features on geology, biology and marine environment are well documented by Judd & Hovland (2007). These seabed depressions are considered geohazards during deep-water exploration and production activities as they may affect subsea installations and must be identified and evaluated (Cauquil and Adamy (OTC 2008); Martinez *et al.,* 2011).

CONCLUSIONS

Based on analysis of 3D reflection seismic data; we divided the post-transform succession into five major seismic units bounded by significant surfaces and major unconformities to investigate depositional and fluid-flow elements along the Nigeria Transform Margin. Conclusions from this study are:

- The overall margin architecture can be attributed to two main sediment sources, the Niger Delta cone feeding the toe set stratigraphy in the eastern study area (Area 1) and the Nigerian Transform Margin feeding sediments southward into the western study area (Area 2.)

- Mass-transport activity along the margin increased through time and is indicative of long-term increasing slope instability within the western part of the study area (Area 2).

- Occurrence of fluid-flow features such as pockmarks, pipes, seabed mound, and BSR are restricted to Area 1, suggesting gas generation was limited to the distal Niger Delta Cone stratigraphy, although a deeper contribution through seal leakage cannot be excluded.

- The relationship between pockmarks, pipes, and BSR with regional, deep-seated faults suggests faults could have acted as migration pathways for upward fluid migration from underlying reservoirs.

- Three (3) main fluid sources are suggested; they include pore water, hydrocarbon from biogenic and thermogenic origin. This needs to be confirmed with additional data such as geochemical data.

- Polygonal faults are present and detected in SU 5 (Pliocene-aged sediments) for the first time ever in offshore Nigeria. These faults have similar dip angles, but smaller throw compared to polygonal faults in the North Sea and Faroe-Shetland basins. They are similar in throw to those interpreted from the Lower Congo basin.

- Results from this study will be useful during exploration and production as mass-transport deposits and fluid flow features could pose potential geohazards on the margin during exploration and production activities and therefore, their location and distribution should be mapped and evaluated in detail at the onset of exploration.

ACKNOWLEDGEMENTS

We wish to thank Petroleum Technology Development Fund (PTDF) Nigeria for proving full scholarship that has made this research possible. We want to thank PGS for providing the 3D seismic volume for this project and their permission to publish. Appreciation also goes to the editor and reviewers for their constructive comments in the process of reviewing this paper.

REFERENCES

ANDRESEN, K.J., CLAUSEN, O.R., HUUSE, M. (2009). A giant (5.3×107 m3) middle Miocene (c. 15 Ma) sediment mound (M1) above the Siri Canyon, Norwegian–Danish Basin: origin and significance. Marine and Petroleum Geology 26, 1640–1655.

ANDRESEN, K.J., HUUSE, M. & CLAUSEN, O.R. (2008). Morphology and distribution of Oligocene and Miocene pockmarks in the Danish North Sea – implications for bottom current activity and fluid migration. Basin Research, 20, 445–46.

ANDREASSEN , K., NILSSEN, E.G. & ØDEGAARD, C.M (2007). Analysis of shallow gas and fluid migration within the Plio-Pleistocene sedimentary succession of the SW Barents Sea continental margin using 3D seismic data. Geo-Marine letter, 27, 155 – 171.

ANDRESEN, K. J (2012). Fluid flow features in hydrocarbon plumbing systems: What do they tell us about the basin evolution? Marine and Petroleum Geology, 26, 1640-1655.

ANSELMETTI, F.S. & EBERLI, G.P (2012). Controls on sonic velocity in carbonates. Pure and Applied Geophysics, 141, 287-323.

BERNDT, C., BÜNZ, S., CLAYTON, T., MIENERT, J., SAUNDERS, M., (2004). Seismic character of bottom simulating reflectors: examples from the mid-Norwegian margin. Marine and Petroleum Geology 21, 723–733.

BLAREZ, E., & MASCLE, J. (1988). Shallow structures and evolution of the Ivory Coast and Ghana transform margin: Marine and Petroleum Geology, 5, 54–64.

BORSATO, R., GREENHALGH, J., MARTIN, M., ZIEGLER, T., MARKWICK, P & QUALLINGTON, A. (2012). Atlantic Conjugate Margin: an exploration strategy. PGS presentation in London.

BORSATO, R., GREENHALGH, J., WELLS, S., ROBERSON, R., & FONTES, C. (?) Prospectivity of the Equatorial Conjugate Margins of Africa and South America: PGS presentation.

BROWNFIELD, M.E., and CHARPENTIER, R. (2006). Geology and total petroleum systems of the Gulf of Guinea province of West Africa: US Geological Survey Bulletin 2207-C, 32.

BULL, S., CARTWRIGHT, C. & HUUSE, M. (2009). A review of kinematic indicators from mass- transport complexes using 3D seismic data. Marine & Petroleum Geology, 26, 1132 – 1151.

CARTWRIGHT, J.A., (1994). Episodic basin-wide hydrofracturing of overpressured early Cenozoic mudrock sequences in the North Sea Basin. Marine and Petroleum Geology 11, 587–607.

CARTWRIGHT, J.A. (2007). The impact of 3D seismic data on the understanding of compaction, fluid flow and diagenesis in sedimentary basins. Journal of the Geological Society, London, 164, 881.

CARTWRIGHT, J.A. (2011). Diagenetically induced shear failure of fine-grained sediments and the development of polygonal fault systems. Marine and Petroleum Geology, 28, 1593 – 1610.

CARTWRIGHT, J., HUUSE, M., APLIN, A., (2007). Seal bypass systems. AAPG Bulletin 91, 1141– 1166.

CATUNEANU, O. (2022). Principles of Sequence Stratigraphy. Second edition, Elsevier.

CAUQUIL, E., & ADAMY, J. (2008). Seabed imagery and chemosynthetic communities: Examples from deep offshore West Africa. Offshore Technology Conference, Houston.

CUNNINGHAM, R., & LINDHOLM, R.M.(2000). Seismic evidence for widespread gas hydrate formation, offshore west Africa. AAPG Memoir 73, 93–105.

DAVIES, R.J. (2003). Kilometer-scale fluidization structures formed during early burial of a deep-water slope channel on the Niger Delta. Geology, 31, 949 - 952.

DAVIES, R.J., & CLARK, I.R. (2006). Submarine slope failure primed and triggered by silica and its diagenesis. Basin Research 18, 339-350.

DAVIES, R. J., HUUSE, M., HURST, P., CATWRIGHT, J. & YANG, Y. (2006). Giant clastic intrusions primed by silica diagenesis. Geology, 34, 917-920.

DYKSTRA, M., FILDANI, A., MOSCARDELLI, L, CLARK, J., GERBER., T & OCHOA, J (2014). Predictive tools for deep-water depositional environments. SEPM workshop, Houston.

GAY, A., LOPEZ, M., BERNT, C., & SERANNE, M. (2007). Geological controls on focused fluid flow associated with seafloor seeps in the Lower Congo Basin: Marine Geology 224, 68-92

GAY, A., LOPEZ, M., COCHONAT, P., SERMONDADAZ, G., (2004). Polygonal faults-furrows sys- tem related to early stages of compaction—upper Miocene to recent sediments of the Lower Congo Basin. Basin Research 16, 101–11

GAY, A., LOPEZ, M., COCHONAT, P., LEVACHÉ, D., SERMONDADAZ, G., SERANNE, M. (2006a). Evidences for early to late fluid migration from an upper Miocene turbiditic channel revealed by 3D seismic coupled to geochemical sampling within seafloor pockmarks, Lower Congo Basin. Marine and Petroleum Geology 23, 387–399.

GAY, A., LOPEZ, M., COCHONAT, P., SÉRANNE, M., LEVACHÉ, D., SERMONDADAZ, G., (2006b). Isolated seafloor pockmarks linked to BSRs, fluid chimneys, polygonal faults and stacked Oligocene–Miocene turbiditic palaeochannels in the Lower Congo Basin. Marine Geology 226, 25– 40.

GAY, A., LOPEZ, M., ONDREAS, H., CHARLOU, J.-L, SERMONDADAZ, G., & COCHONAT, P., (2006c). Seafloor facies related to upward methane flux within a Giant pockmark of the Lower Congo Basin. Marine Geology 226, 81-95.

GAY, A., LOPEZ, M., COCHONAT, P., SULTAN, N., CAUQUIL, E., & BRIGAUD, F (2003). Sinuous pockmark belt as indicator of a shallow buried turbiditic channel on the lower slope of the Congo basin, West African margin. In: Van Rensbergen, P., Hillis, R.R. & Morley, C.K. (eds) Subsurface Sediment Mobilization. Geological Society, London, Special Publications, 216, 173–189.

GEE, M.J.R & GAWTHORPE, R.L (2007). Early evolution of submarine channels offshore Angola revealed by three-dimensional seismic data. Geological Society of London, Special Publication, 27, 223-235

GOULTY, N.R (2001). Polygonal fault networks in fine-grained sediments an alternative to the syneresis mechanism. First break 19, 69-73

GRAUE, K., (2000). Mud volcanoes in deepwater Nigeria. Marine and Petroleum Geology 17, 959–974

GREENHALGH, J., WELLS, S., BORSATO,. R., PRATT, D., MARTIN, M., ROBERSON., R., FONTES., & OBAJE, W.A. (2011). A fresh look at prospectivity of the Equatorial Conjugate Margin of Brazil and Africa. First Break, 29, 67-72

GREVEMEYER, I & VILLINGER, H (2001). Gas hydrate stability and the assessment of heat flow through continental margins. Geophysical Journal International, 145, 3, 647-660

HEGGLAND, R., (1998). Gas seepage as an indicator of deeper prospective reservoirs. A study based on exploration 3D seismic data. Marine and Petroleum Geology 15, 1–9.

HO, S., CATWRIGHT, J & IMBERT, P. (2012). Vertical evolution of fluid venting structures in relation to gas flux, in the Neogene-Quaternary of the Lower Congo Basin, Offshore Angola. Marine Geology, 332-334, 40-55.

HOVLAND, M. (2005). Gas hydrates. Petroleum geology, 4, 261 – 268.

OFFICIAL

HOVLAND, M., JUDD, A.G. 1988). Seabed Pockmarks and Seepages: Impact on Geology, Biology and the Marine Environment.

HUSTOFT, S., BÜNZ, S., MIENERT, J. (2010). Three-dimensional seismic analysis of the morphology and spatial distribution of chimneys beneath the Nyegga pockmark field, offshore mid- Norway. Basin Research 22, 465–480.

HUUSE, M., JACKSON, C.A.-L., RENSBERGEN, P. V., DAVIES, R.J., FLEMINGS, P.B. & DIXON, R.J. (2010). Subsurface sediment remobilization and fluid flow in sedimentary basins: an overview: Basin Research, 22, 342-360.

JUDD, A., HOVLAND, M. (2007). Seabed fluid flow - the impact on geology, biology and the marine environment. Cambridge University Press, 475.

Klaucke, I., Sarkar, S., Bialas, J., Berndt, C., Dannowski, A., Dumke, I., et al. (2018). Giant depressions on the Chatham Rise offshore New Zealand – morphology, structure and possible relation to fluid expulsion and bottom currents. Mar. Geol. 399, 158–169. doi:10.1016/j.margeo.2018.02.011.

KILHAMS, B., MCARTHUR, A., HUUSE, M., ITA, E., HARTLEY, A., (2011). Enigmatic large-scale furrows of Miocene to Pliocene age from the central North Sea: current-scoured pockmarks? Geomarine Letters 31, 437–449.

KING, L.H., MACLEAN, B. (1970). Pockmarks on the Scotian Shelf. Geological Society of American Bulletin 81, 3141–3148.

LIGTENBERG, J.H. (2005). Detection of fluid migration pathways in seismic data: implications for fault seal analysis. Basin Research, 17. 141-153.

LONERGAN, L., CARTWRIGHT, J. & JOLLY, R. (1998). The geometry of polygonal fault systems in Tertiary mudrocks of the North Sea. Journal of the Geological Society, 83, 529-548.

LONERGAN, L., & CARTWRIGHT, J. (1999). Polygonal faults and their influence on deep-water depositional sandstone reservoir geometries , Alba Field United Kingdom Central North Sea. AAPG Bulletin 83, 410–432.

LØSETH, H., WENSAAS, L., ARNTSEN, B., HANKEN, N., BASIRE, C., GRAUE, K., (2001). 1000 m long gas blow-out pipes. 3rd EAGE Conference & Exhibition, Amsterdam, Extended Abstracts, 524.

LØSETH, H., GADING, M., WENSAAS, L. (2009). Hydrocarbon leakage interpreted on seismic data. Marine and Petroleum Geology 26, 1304–1319.

LØSETH, H., WENSAAS, L., ARNTSEN, B., HANKEN, N., BASIRE, C., GRAUE, K. (2011). 1000 m long gas blow-out pipes. Marine and Petroleum Geology 27, 1047–1060.

MACGREGOR, D.S., ROBINSON, J., AND SPEAR, G. (2003). Play fairways of the Gulf of Guinea transform margin, in Arthur, T.J., MacGregor, D.S., and Cameron, N.R., eds., Petroleum geology of Africa—New themes and developing technologies: Geological Society, London, Special Publication 207, 289.

MARTINEZ, J.F., CARTWRIGHT, J., HALL, B. (2005). 3D seismic interpretation of slump complexes: examples from the continental margin of Israel. Basin Research 17,83–108.

MARTÍNEZ, J.F., BERTONI, C., GÉRARD, J., & MATÍAS, H. (2011). Processes of submarine slope failure and fluid migration on the Ebro continental margin: implications for offshore exploration and development In: Shipp, R.C., Weimer, P., & Posamentier, H.W. (eds). Mass transport deposits in deep-water settings. SEPM Special Publication 96, 181-198

MECKEL, L. D (2011). Reservoir characteristics and classification of sand-prone submarine mass-transport deposits. In: Shipp, R.C., Weimer, P., & Posamentier, H.W. (eds). Mass transport deposits in deep-water settings. SEPM Special Publication 96, 423-45266.

MITCHUM JR., R.M., VAIL, P.R., SANGREE, J.B. (1977). Seismic stratigraphy and global changes of sea-level, part 6: stratigraphic interpretation of seismic reflection patterns in de- positional sequences.

In: Payton, C.E. (Ed.), Seismic Stratigraphy—Applications to Hydrocarbon Exploration: AAPG Memoir, 26, 117–133.
MOSCARDELLI, L.,WOOD, L.&MANN, P. (2006). Mass-transport complexes and associated processes in the Offshore Area of Trinidad and Venezuela. AAPG Bulletin, 90, 1059-1088.
MOSCARDELLI, L. & WOOD, L. (2008). New classification system for mass transport complexes in offshore Trinidad. Basin Research 20, 73 – 98.
MOSS, J.L., CARTWRIGHT, J., (2010). The spatial and temporal distribution of pipe formation, offshore Namibia. Marine and Petroleum Geology 27, 1216–1234.
NELSON, C.H., ESCUTIA, C., DAMUTH., J.E., & TWICHELL (Jr), D.C. (2011). Interplay of mass-transport and turbidite-system deposits in different active tectonic and passive continental margin settings: external and local controlling factors. In: Shipp, R.C., Weimer, P., & Posamentier, H.W. (eds). Mass transport deposits in deep-water settings. SEPM Special Publication 96, 39-66.
NISSEN, S.E., HASKELL, N.L., STEINER, C.T., COTERILL, K.L., (1999). Debris flow outrunner blocks, glide tracks, and pressure ridges identified on the Nigerian continental slope using 3-D seismic coherency. The Leading Edge 18, 595–599.
OBAJE, N.G. (2009). The Dahomey Basin. Geology and Mineral Resources of Nigeria, Lecture Notes in Earth Sciences 120, 103-108.
OSTANIN, I., ANKA, Z., DI PRIMIO, R., BERMAL, A., (2012) Hydrocarbon leakage above the Snøhvit gas field, Hammerfest Basin SW Barents Sea. First Break, 30, 55-6.
PETROLEUM GEO-SERVICES (2006). Techlink, a PGS Geophysical, 6, 2.
PILCHER, R., ARGENT, J. (2007). Mega-pockmarks and linear pockmark trains on the West African continental margin. Marine Geology 244, 15–32.
POSAMENTIER, H. W & KOLLA, V. (2003). Seismic geomorphology and stratigraphy of depositional elements in deep-water settings. Journal of Sedimentary Research, 73, 3, 367 – 388.
POSAMENTIER, H. W & MARTINSEN, O.J (2011). The character and genesis of submarine mass-transport deposits: insights from outcrop and 3d seismic data. In: Shipp, R.C., Weimer, P., & Posamentier, H.W. (eds). Mass transport deposits in deep-water settings. SEPM Special Publication 96, 7-38.
REICHE, S., HJELSTUEN, B.O & HAFLIDASON. H (2011). High-resolution seismic stratigraphy, sedimentary processes and the origin of seabed cracks and pockmarks at Nyegga, mid-Norwegian margin. Marine Geology, 284, 28-39.
RISE, L., SÆTTEM, J., FANAVOLL, S., THORSNES, T., OTTESEN, D., BØE, R., (1999). Sea-bed pockmarks related to fluid migration from Mesozoic bedrock strata in the Skagerrak offshore Norway. Marine and Petroleum Geology 16, 619–631.
SCHROOT, B.M. & SCHÜTTENHELM, R.T.E. (2003). Expressions of shallow gas in the Netherlands North Sea. Netherlands Journal of Geosciences, 82, 91-105.
SERIÉ, C., HUUSE, M., SCHØDT, N. (2012). Gas hydrate pingoes: deep seafloor evidence of focused fluid flow on continental margins. Geology 40, 207–210.
SHIPLEY, T.H., HOUSTON, M.,H., BUFFLER, R.T., SHAUB, F.J., McMILLEN, K.J., LADD,J.W., and WORZEL, J.L. (1979). Seismic evidence of widespread possible gas hydrate horizons on continental slopes and rises: AAPG Bulletin, 63, 2204-2213.
SHIPP, R.C., WEIMER, P., & POSAMENTIER, H.W. (2011). Mass transport deposits in deep-water settings: an introduction. In: Shipp, R.C., Weimer, P., & Posamentier, H.W. (eds). Mass transport deposits in deep-water settings. SEPM Special Publication 96, 3-6.
SHOULDERS, S.J., CARTWRIGHT, J. & HUUSE, M. (2007). Large scale conical sandstone intrusions and polygonal fault systems in Tranche 6, Faroe-Shetland basin. Marine & Petroleum Geology, 24, 173-188.

STEWART, S.A. (1999). Seismic interpretations of circular geological structures. Petroleum Geoscience, 5, 273-285.

STUEVOLD, L.M., FAERSETH, R.B., ARNESEN, L., CARTWRIGHT, J. & MO¨LLER, N. (2003). Polygonal faults in the Ormen Lange Field, Møre Basin, offshore Mid-Norway. In: Van Rensbergen, P., Hillis, R.R. & Morley, C.K. (eds) Subsurface Sediment Mobilization. Geological Society, London, Special Publications, 216, 263–281.

SULTAN, N., MARSSET, B., KER, S., MARSSET, T., VOISSET, M., VERNANT, A.M., BAYON, G., CAUQUIL, E., ADAMY, J., COLLIAT, J.L., DRAPEAU, D., (2010). Hydrate dissolution as a potential mechanism for pockmark formation in the Niger delta. Journal of Geophysical Research, 113, 1 – 33.

SUTTON, J.P., & MITCHUM, R.M. Jr (2011). Upper Quaternary seafloor mass-transport deposits at the base of slope, offshore Niger Delta, deep-water Nigeria. In: Shipp, R.C., Weimer, P., & Posamentier, H.W. (eds). Mass transport deposits in deep-water settings. SEPM Special Publication 96, 85-110.

VANNESTE, M., MIENERT, J., BUNZ, S. (2006). The Hinlopen Slide: A giant, submarine slope failure on the northern Svalbard margin, Arctic Ocean. Earth and Planetary Science Letters 245, 373–388.

VAN RENSBERGEN, P., HILLIS, R.R., MALTMAN, A.J., MORLEY, C.K. (Eds.), (2003a) Subsurface Sediment Mobilization: Geological Society Special Publications, Geological Society, London, Special Publications, 216.

Waghorn, K.A., Pecher, I., Strachan, L.J., Crutchley, G., Bialas, J., Coffin, R.B., Davy, B., Koch, S., Kröger, K.F., Papenberg, C., Sarkar, S., (2018). SO226 Scientific Party, Paleo-fluid expulsion and contouritic drift formation on the Chatham Rise, New Zealand, Basin Res., 30, pp. 5-19, 10.1111/bre.12237

ZHU, M., GRAHAM.S., & McHARGUE, T. (2011). Characterization of mass-transport deposits on a Pliocene siliciclastic continental slope, North western South China Sea. In: Shipp, R.C., Weimer, P., & Posamentier, H.W. (eds). Mass transport deposits in deep-water settings. SEPM Special Publication 96, 111-125.

ZIEGLER, P.A. ed. (1988) Evolution of the Arctic-North Atlantic and the Western Tethys. The American Association of Petroleum Geologists, Tulsa, OK, USA. AAPG Memoir 43.

FIGURES AND TABLE CAPTIONS

Fig. 1(a) *Gulf of Guinea Province (7183) with location of oil and gas fields shown in red outline;* ***(b)*** *Structural zones along the West African transform Margin and location of study area. The area covers OPL blocks 300, 301 and 302 as shown in red. Yellow and blue boxes represent location of soft-sediment deformation features and fluid flow pipes by Davies 2003 & Løseth et al., 2011, respectively. Aje field and Ogo discoveries also shown by the black circles in the upper left. Area falls within the frontal deformation zone. Inset shows location of study area within the Atlantic (Redrawn from Brownfield & Charpentier 2006; Techlink, PGS 2006).*

Fig. 2*. Simplified stratigraphic column and petroleum systems along the West African Transform Margin (adapted from Borsato et al., 2012). Also shown is the occurrence of MTDs and fluid flow features observed from the study area from this study. Green squares labelled S on the image represents location of source rocks.*

Fig. 3 *TWT structure map of the seabed topography showing the extent of the 3D seismic data used for study. Entire study area is divided into 2 areas for ease of description and discussion. Division is based on approximate extent of MTDs and fluid flow deposits (depth range c. 1350-2700 m).*

***Fig. 4a**. Dip line across the study area showing major surfaces and units. Surfaces extended from Aje field towards the northern part of the survey (PGS). Location of line shown on seabed map**; 4b-e.** Strike and random dip lines across the study area showing seismic units and surfaces. Units are defined based on seismic facies and terminations. SU2 to SU5 are extensively deformed units with the MTDs. The blocked out part of the seismic (yellow/white) is due to commercially sensitive data and not provided by data owners, PGS.*

***Fig. 5. (a-e)** TWT thickness maps of the mapped seismic units.*

***Fig. 6** Dip angle and variance attribute maps to show a 3D perspective view of the topography of the seabed. Depositional, soft-sediment deformation and fluid flow features such as, submarine channels, sediment waves, mass transport deposits, pockmarks and mound are well imaged using the variance attribute with red indicating areas of topographic highs and channel margins.*

***Fig. 7** Summary diagrams of key components of the mass transport deposits along the Nigeria Transform Margin often used for kinematic indication. The figure is split into the three domains related to MTD; the . headwall , translational and toe domains. The variance maps help to image the lateral extent, margins and internal geometries of the MTDs. It shows a sharp contrast along the margins. The longitudinal shear is best images with the RMS attribute map with the blues representing the shear zones and the purple the surrounding under deformed background. Deformed blocks within the translational domain were imaged cleared from the TWT maps with the reds representing the positive topography as result of the deformation.*

***Fig 8.** Mass transport deposits in the area **(a)** seafloor topography as shaded relief map showing components of a series of mass transport deposits. At least three are identified. Image also reveals other seafloor features such as meandering and straight channels, pockmarks, faults and a mound. Red arrow shows transport direction of failed sediments moving south; **(b)** seismic section through the headwall scarp of MTD 2. Note how fault cuts through the sediments; **(c)** dip seismic line revealing all three MTDs on the seafloor. Headwall scarps and lateral margins are well imaged. High-amplitude reflections observed directly beneath the seabed and above the faulted structural high. Line locations for b and c shown on a.*

***Fig. 9. (a&b)** Seismic profile showing well- preserved, deformed MTD blocks and other features; **(c)** variance extracted on top surface of deformed blocks **(d)** time structure map of base of SU5 showing MTD ramps; (e) TWT ms map through the ramp shown in figs a & b. The ramp cuts through ~250 TWT ms of stratigraphy and up to 5 Km wide.*

***Fig. 10** Evolution and distribution of MTDs along the Nigerian Transform Margin during the Cenozoic. Coloured patches represent single MTD drawn from its basal surface. Deformation became more frequent through time. Note that outline of seabed MTDs are not include*

***Fig 11**. Iso-proportional slicing through a frequency decomposition RGB colour blend volume. Each of the colours correspond to a given frequency through the channel with a distinct amplitude response. Where the frequency has a very strong response, it is represented as white, light brown or grey to light grey areas; which reflects the main channel complexes. Where the frequency gives a weak response, it is represented as dark or black colours, which reflects the non-channelised surrounding units. **(a)** W-E seismic section showing location of slices (time 10 – time 1) from the seabed to the*

base of the channel complexes, Cc; ***(b)*** *individual iso-slice to image channels. At least five channel complexes/belts are observed. Cc1 is meandering and confined within the belt but Cc2 – 4 are not. Cc5 forms a linear channel complex belt. Note location of seabed mound above paleo channels. MTDs are also observed.*

Fig. 12. (a & b) *TWT surface and RMS attribute map of the seabed to image linear channels in 3D view. Channels react near structural high; they merge and bifurcate downslope forming two more channels;* ***(c-f)*** *seismic profiles downslope across channels* ***(g)*** *dip map of the seabed showing the linear channels in 3D view*

Fig. 13. *Sediment waves.* ***(a)*** *RMS amplitude map at 50 ms TWT below the present day seabed showing morphology of sediment waves. Transport direction is northeast to southwest;* ***(b)*** *cross section through the train of sediment wave;* ***(c & d)*** *dip and random lines showing how the reflections interpreted as sediment waves are constrained within the channel margin. Note presence of polygonal faults. Location of lines shown in "a"*

Fig. 14*. Isolated pipes and pockmarks above a structural high in the northern part of the study area.* ***(a)*** *seismic section through vertical columns and depressions on the seafloor interpreted as pipes and pockmarks respectively. Inset shows the circular to oval geometry of the pockmarks from the time slice taken at -1808 ms;* ***(b)*** *Dip amplitude map of the seafloor reveals the distribution of pockmarks;* ***(c-g)*** *isolated pockmarks and underlying pipe anomalies. Locations shown in b. Note the occurrence of high- amplitude anomalies below pipes, along fault planes and above structural.*

Fig.15*. Seismic expression of pockmarks.* ***(a)*** *stacked pockmarks and schematic diagram;* ***(b)*** *surface of individual level of stacked pockmarks. Note how it deepens and widens with depth;* ***(c)*** *another example of stacked pockmarks;* ***(d - f)*** *pockmarks associated with fault,* ***(d)*** *above the fault plane* ***(e)*** *along hanging wall of fault;* ***(f)*** *TWT and attribute maps on the seabed showing plan-view expression of pockmarks and faults. These features are visible when imaged using different attribute maps such as dip attribute (fiii); black/white scale of the TWT map and variance map iii &(fv).*

Fig. 16 *Presence of pockmarks above active and palaeochannels.* ***(a)*** *variance attribute extracted on the present day seabed. Pockmarks (red arrows) are randomly distributed within the present day channel-belt complex and above paleochannels. Location of seismic sections shown;* ***(b)*** *line through the main channel-belt complex. Pockmarks occur above channel margins;* ***(c)*** *seismic line across the main channel-belt. Pockmarks occur within and away from it;* ***(d & e)*** *pockmarks on the seabed above paleochannels. Fluids could have migrated through porous sands within the channels or along faults to the seabed to create pockmarks*

Fig. 17*.* ***(a)*** *3D image with seismic cross section and RMS attribute extracted on the yellow horizon with a window length of 25 ms to reveal circular and elongate plan view geometries of high-amplitude, wedge-shaped anomalies;* ***(b)*** *profile through isolated pockmarks;* ***(c)*** *plan-view geometry showing relationship between circular and elongated pockmarks and location of seismic profiles;* ***(d)*** *Seismic profile in 16a showing relationship between the deep-seated, regional faults and high-amplitude, wedge-shaped anomalies. Shallow interval also affected by polygonal faults. Inset shows*

transition from circular pockmark to elongated pockmarks due to fault interaction. Note presence of BSR.

***Fig. 18a&b**. Seismic and interpreted section showing BSR; **(c&d)** pockmarks occur above BSR and interval is polygonally faulted. Note presence of free gas below; **(e)** 3D image showing relationship between BSR and faults in the area. BSR (black lines) were mapped only on lines where they clearly crosscut the stratigraphy*

***Fig.19**. Seabed mound/ **(a)** variance extraction on the seabed showing mound and other seafloor features; **(b)** dip seismic line across the mound. Vertical column with distorted internal facies below the mound. Surrounding strata are unaffected by distortion; **(c)** strike seismic line across the mound. High-amplitude intervals below the vertical column are paleo or buried channels; **(d)** 3D image illustrating the relationship between the mound, underlying vertical column and sand-filled channels; **(e)** time slices at -2380, -2392 and -2404 ms TWT through the vertical column.*

***Fig 20. (a)** Seismic profile showing presence of polygonal faults networks with SU3-5; **(b)** seismic amplitude map of the green horizon showing polygonal geometry of the faults from Paleoscan; **(c&d)** close up of seismic line in (a) and variance (trace to trace discontinuity) attribute on the green horizon. F1 and F2 are used to represent the normal faults in the area. Note how the faults are better imaged using variance. Polygonal fault orientation changes close to the major regional faults; **(e)** time structure map; and **(f)** variance attribute from the shallower section showing polygonal faults.*

***Fig. 21** Summary of depositional, soft-sediment remobilisation/deformation and fluid flow elements observed along the Nigerian Transform Margin.*

***Fig. 22 (a)** variance on seabed; **(b-j)** schematic representations of seabed and overburden fluid flow features observed in Area 1. Inset shown to zoom in on Area 1 to show fluid flow features on the seabed*

***Fig. 23** Graphical representation of estimated net sediment accumulation rate in Area 1. Inset diagram represents spatial distribution of mass transport deposits in the area*

***Table 1** Key seismic data parameters such as frequency, velocity, horizontal and vertical resolution for each of the seismic units.*

***Table 2** Similarities and differences between polygonal faults in this study and other basins*

***Table 3** Estimated net sediment accumulation rates of Cretaceous till present day in NTM*

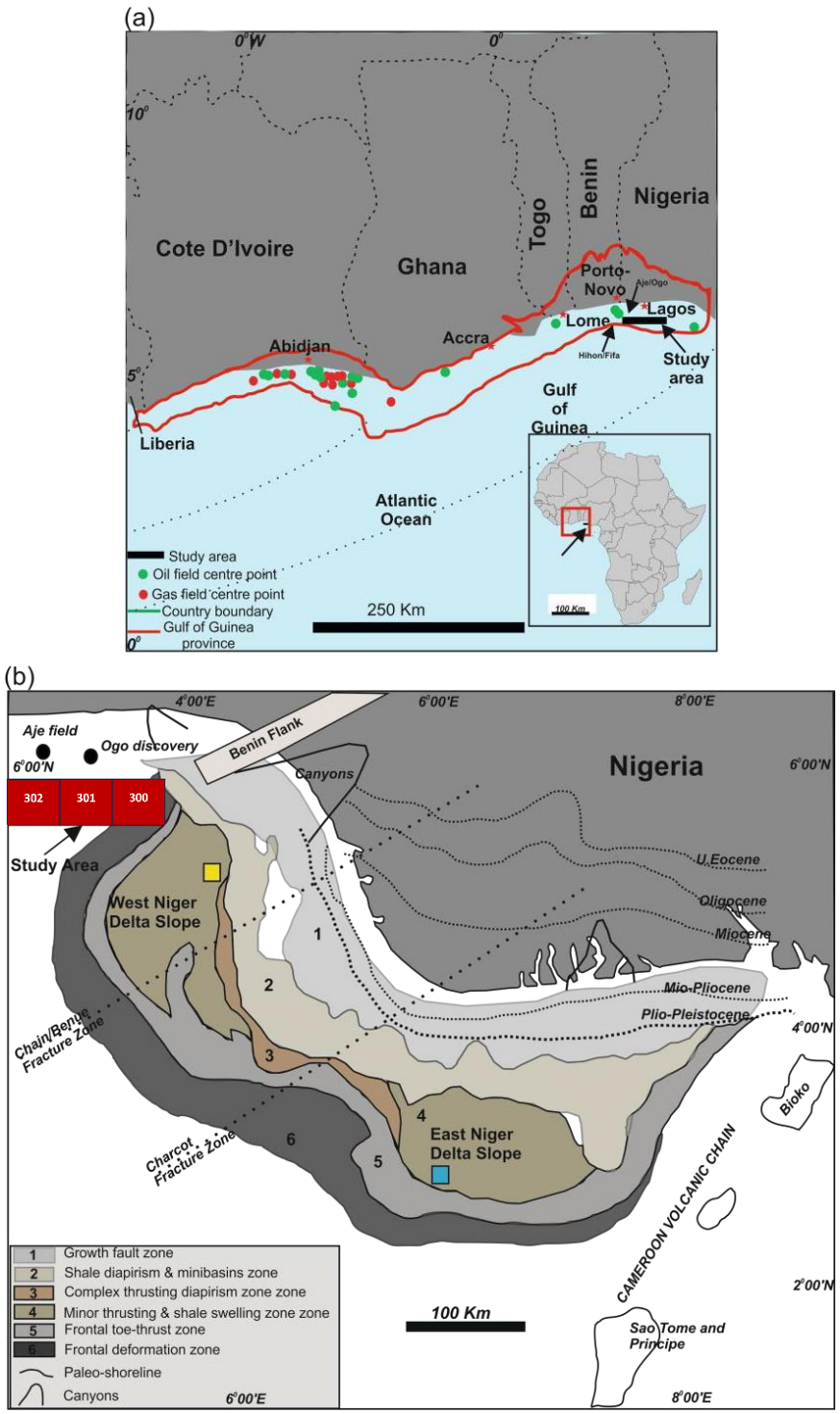
(a)
0°W
0°
10°
5°
0°
Cote D'Ivoire
Ghana
Togo
Benin
Nigeria
Porto-Novo
Aje/Ogo
Lagos
Lome
Accra
Abidjan
Hihon/Fifa
Study area
Gulf of Guinea
Liberia
Atlantic Ocean
Study area
Oil field centre point
Gas field centre point
Country boundary
Gulf of Guinea province
250 Km
100 Km
(b)
4°00'E
6°00'E
8°00'E
Aje field
Ogo discovery
6°00'N
Benin Flank
Canyons
Nigeria
302
301
300
Study Area
West Niger Delta Slope
U.Eocene
Oligocene
Miocene
Mio-Pliocene
Plio-Pleistocene
Chain/Benue Fracture Zone
Charcot Fracture Zone
East Niger Delta Slope
Bioko
CAMEROON VOLCANIC CHAIN
Sao Tome and Principe
1 Growth fault zone
2 Shale diapirism & minibasins zone
3 Complex thrusting diapirism zone zone
4 Minor thrusting & shale swelling zone zone
5 Frontal toe-thrust zone
6 Frontal deformation zone
Paleo-shoreline
Canyons
100 Km

Fig 1.

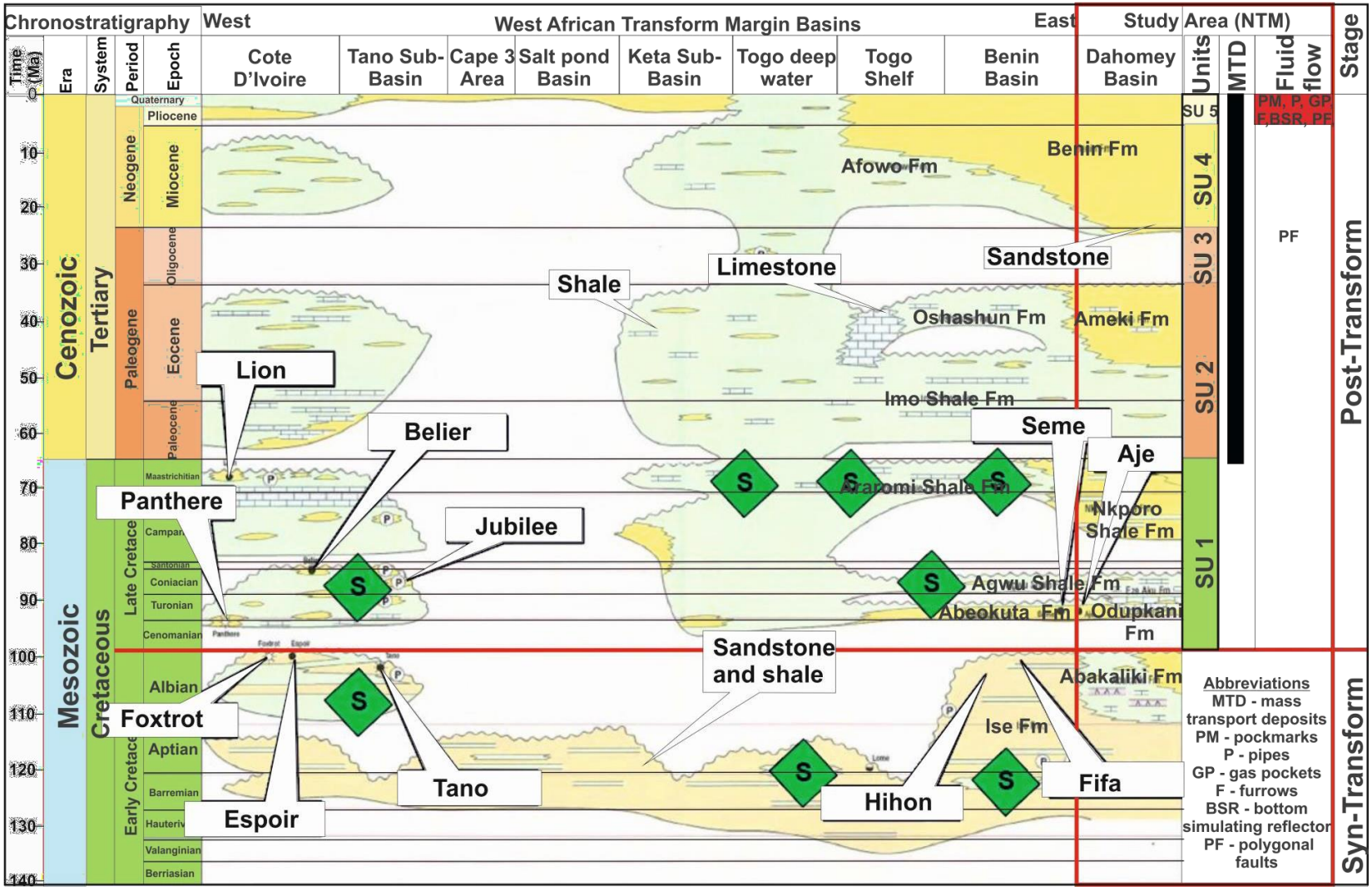

Fig 2.

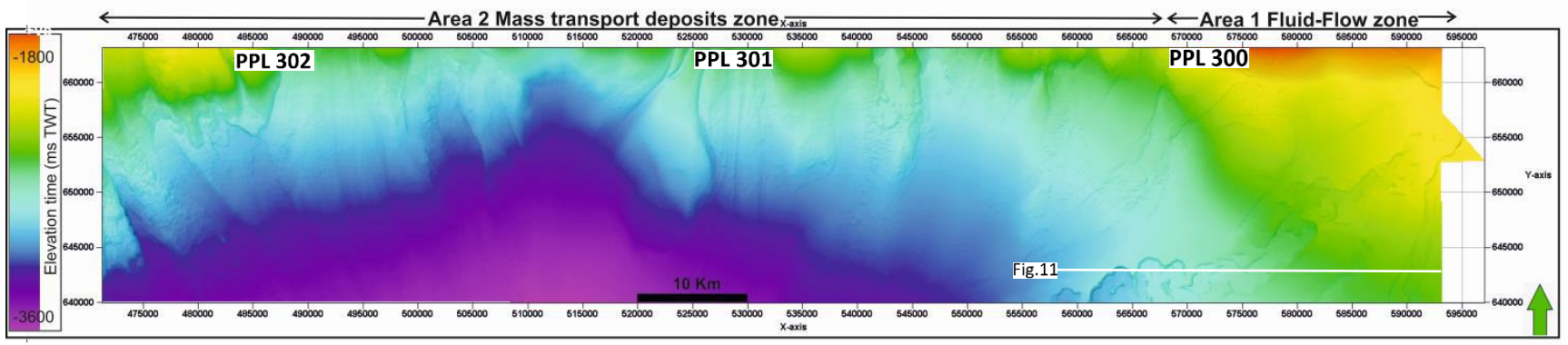
Area 2 Mass transport deposits zone
Area 1 Fluid-Flow zone
PPL 302
PPL 301
PPL 300
-1800
-3600
Elevation time (ms TWT)
10 Km
Fig.11
X-axis
Y-axis

Fig. 3

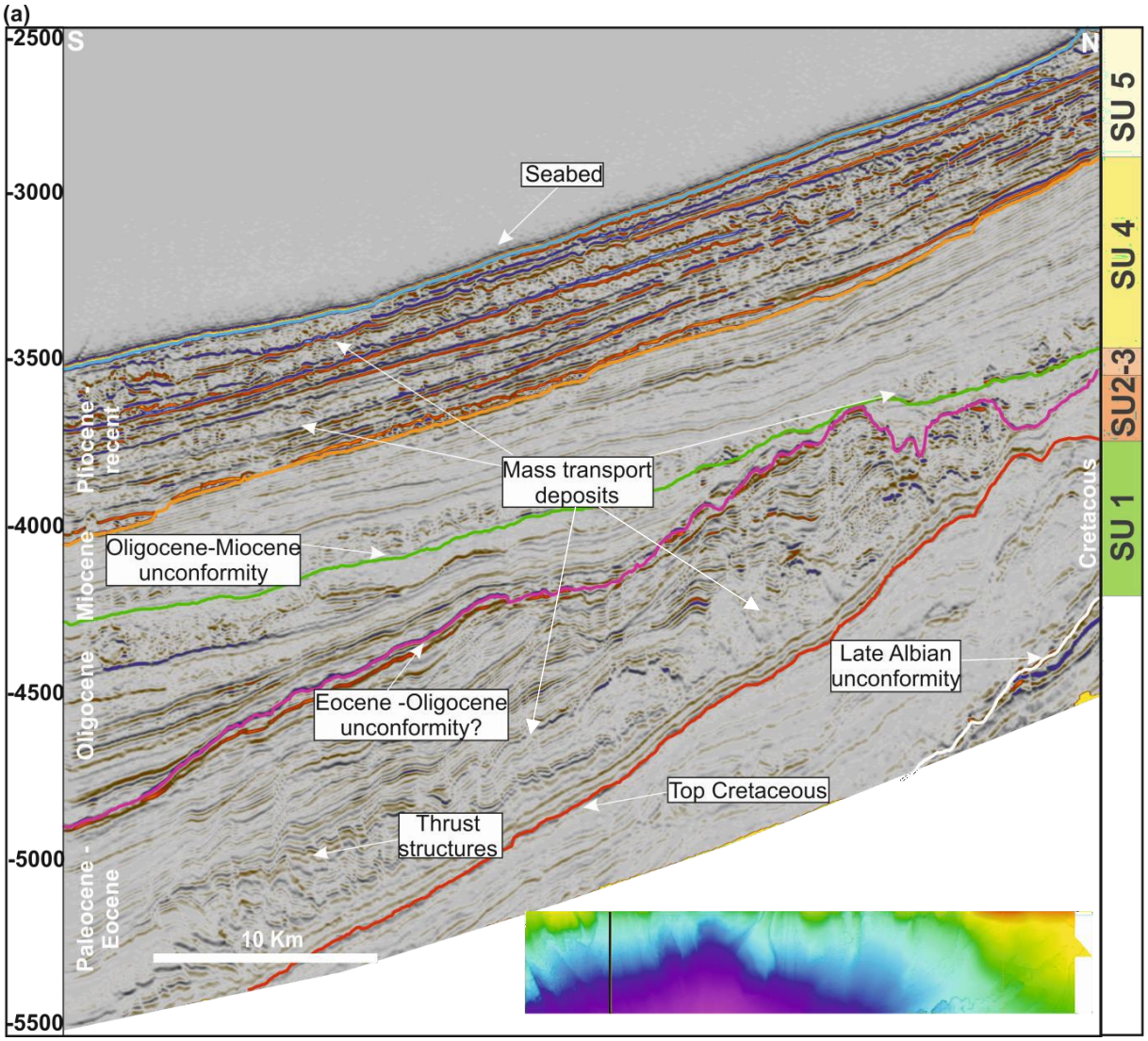

Fig. 4a.

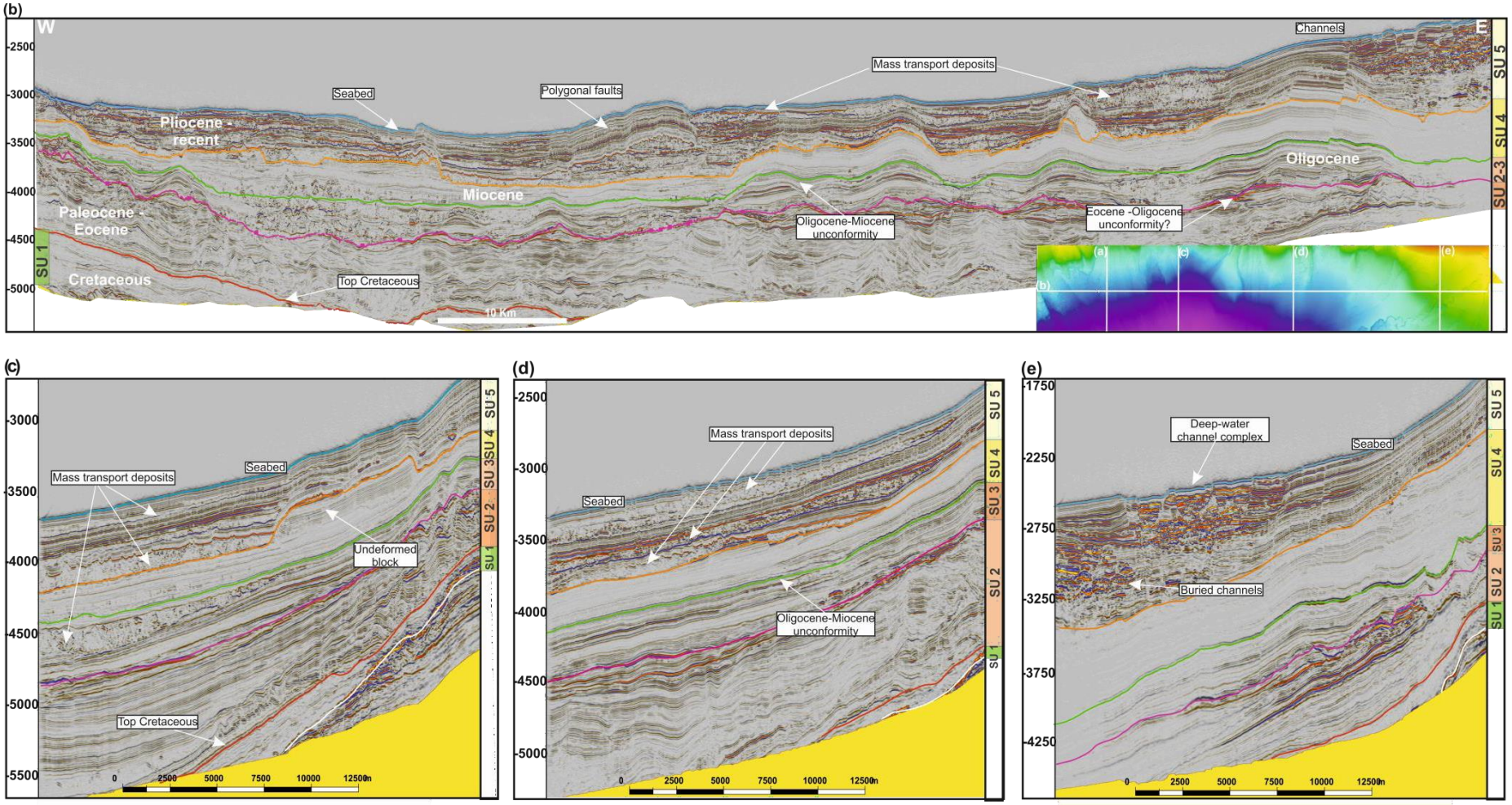
(b)
W
E
Channels
Mass transport deposits
Seabed
Polygonal faults
Pliocene - recent
Miocene
Oligocene
Paleocene - Eocene
Oligocene-Miocene unconformity
Eocene -Oligocene unconformity?
Cretaceous
Top Cretaceous
10 Km
SU 1
SU 2-3
SU 4
SU 5
(c)
Mass transport deposits
Seabed
Undeformed block
Top Cretaceous
(d)
Mass transport deposits
Seabed
Oligocene-Miocene unconformity
(e)
Deep-water channel complex
Seabed
Buried channels
0 2500 5000 7500 10000 12500m

Fig. 4b-e.

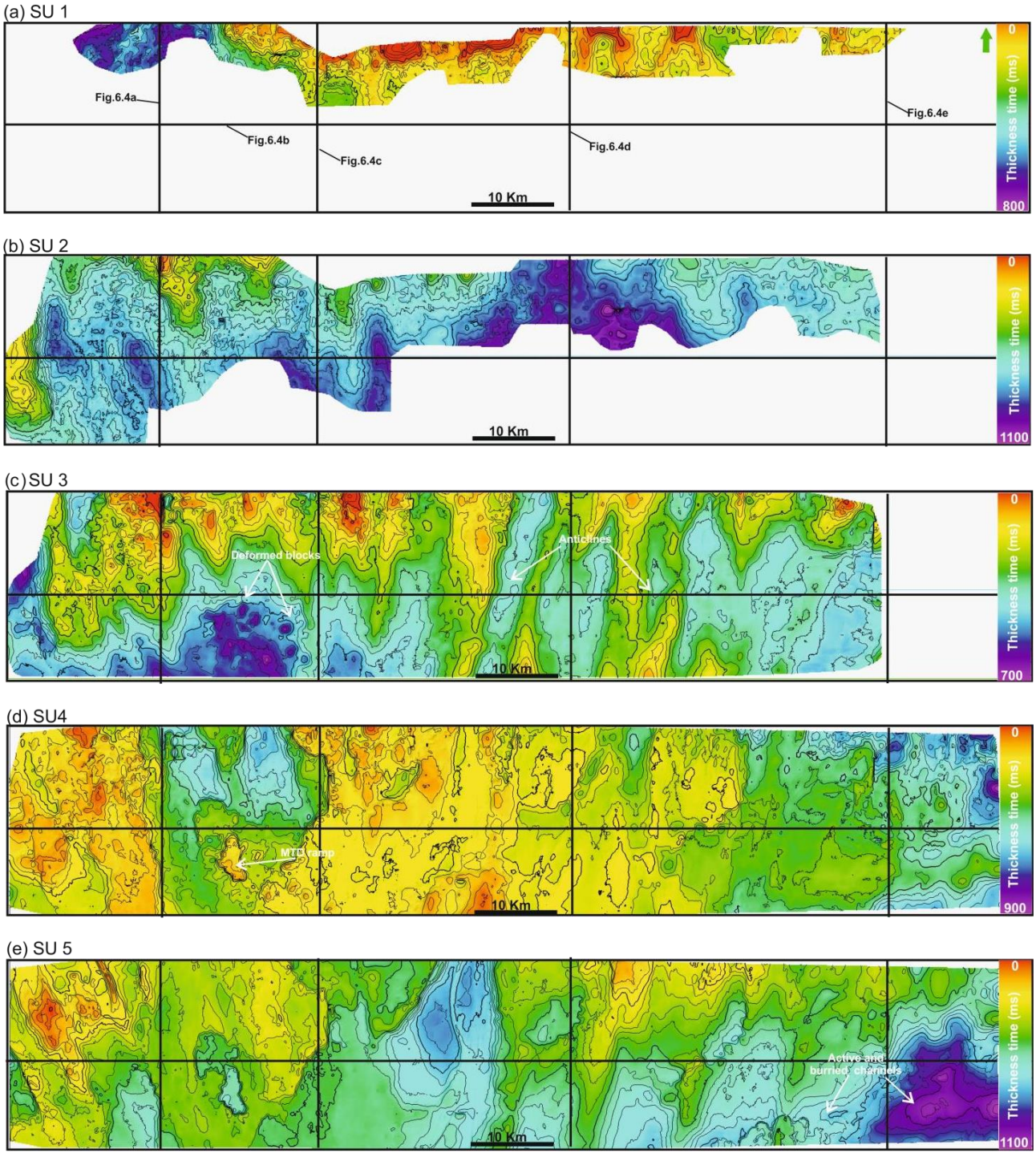
(a) SU 1
Fig.6.4a
Fig.6.4b
Fig.6.4c
Fig.6.4d
Fig.6.4e
10 Km
Thickness time (ms)
0
800
(b) SU 2
10 Km
Thickness time (ms)
0
1100
(c) SU 3
Deformed blocks
Anticlines
10 Km
Thickness time (ms)
0
700
(d) SU4
MTD ramp
10 Km
Thickness time (ms)
0
900
(e) SU 5
Active and buried channels
10 Km
Thickness time (ms)
0
1100

Fig. 5.

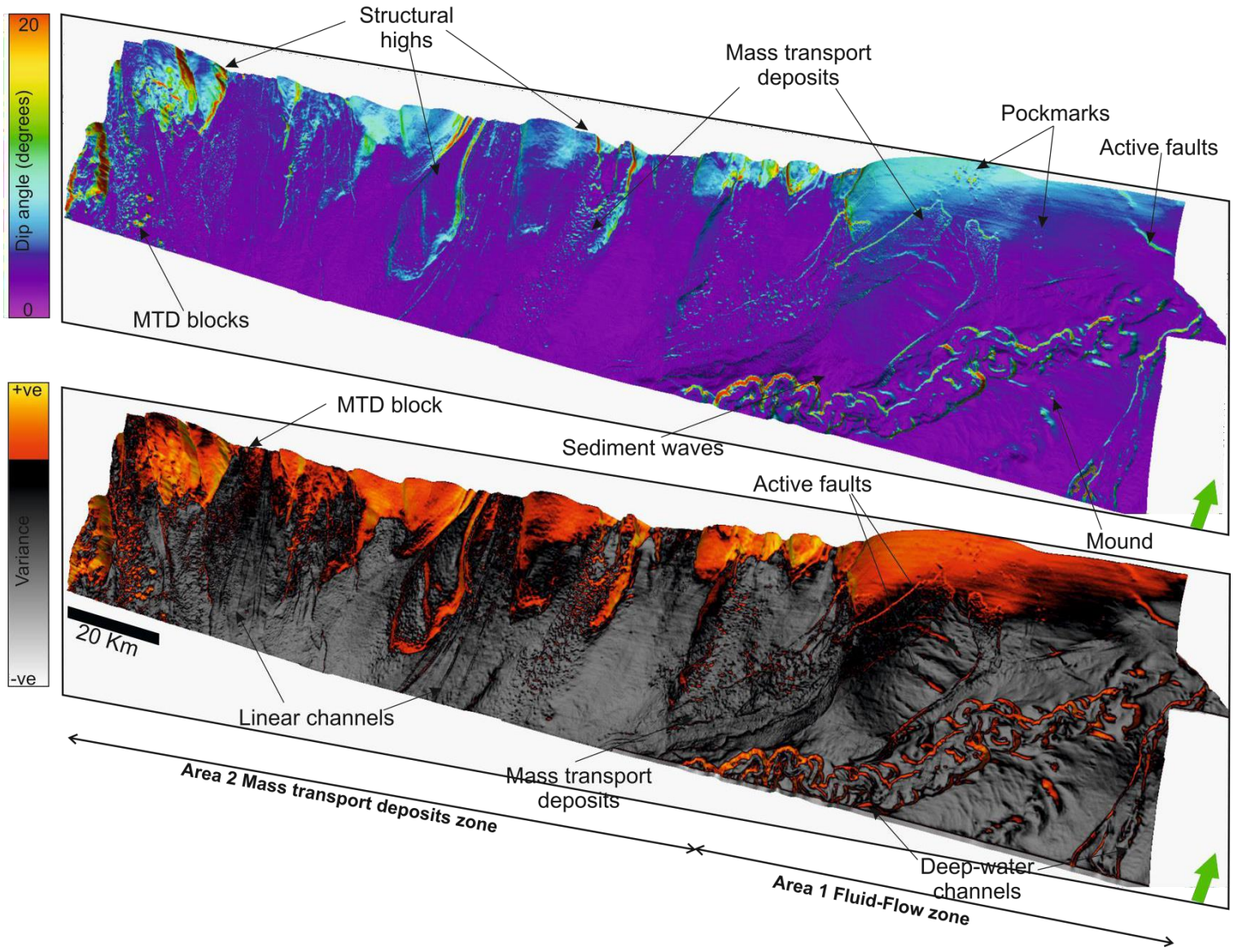

Fig. 6

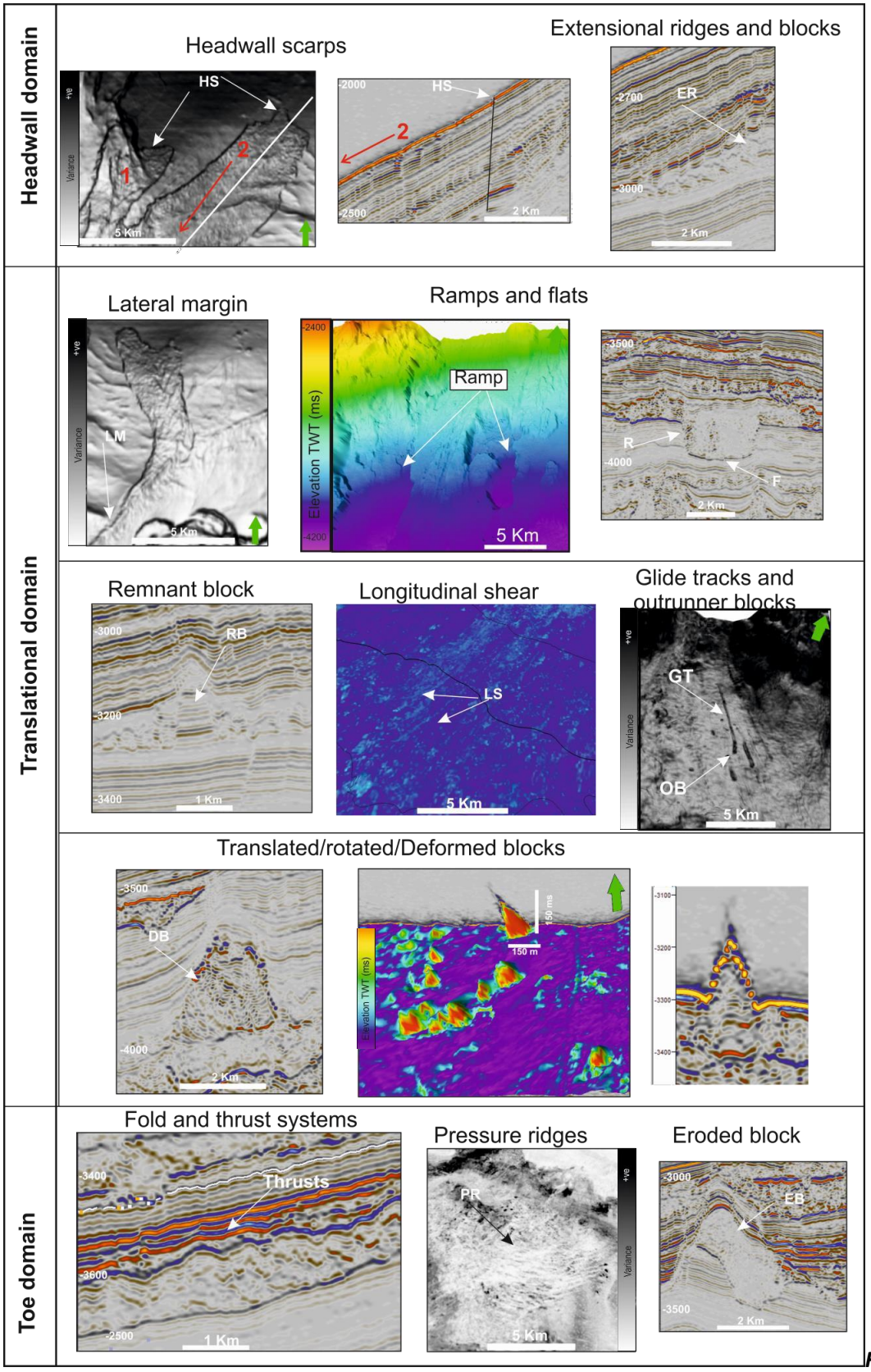
Headwall domain
Translational domain
Toe domain
Headwall scarps
HS
1
2
5 Km
HS
2
2 Km
Extensional ridges and blocks
ER
2 Km
Lateral margin
LM
5 Km
Ramps and flats
Ramp
Elevation TWT (ms)
5 Km
R
F
2 Km
Remnant block
RB
1 Km
Longitudinal shear
LS
5 Km
Glide tracks and outrunner blocks
GT
OB
5 Km
Translated/rotated/Deformed blocks
DB
2 Km
150 m
Elevation TWT (ms)
Fold and thrust systems
Thrusts
1 Km
Pressure ridges
PR
5 Km
Eroded block
EB
2 Km

Fig. 7

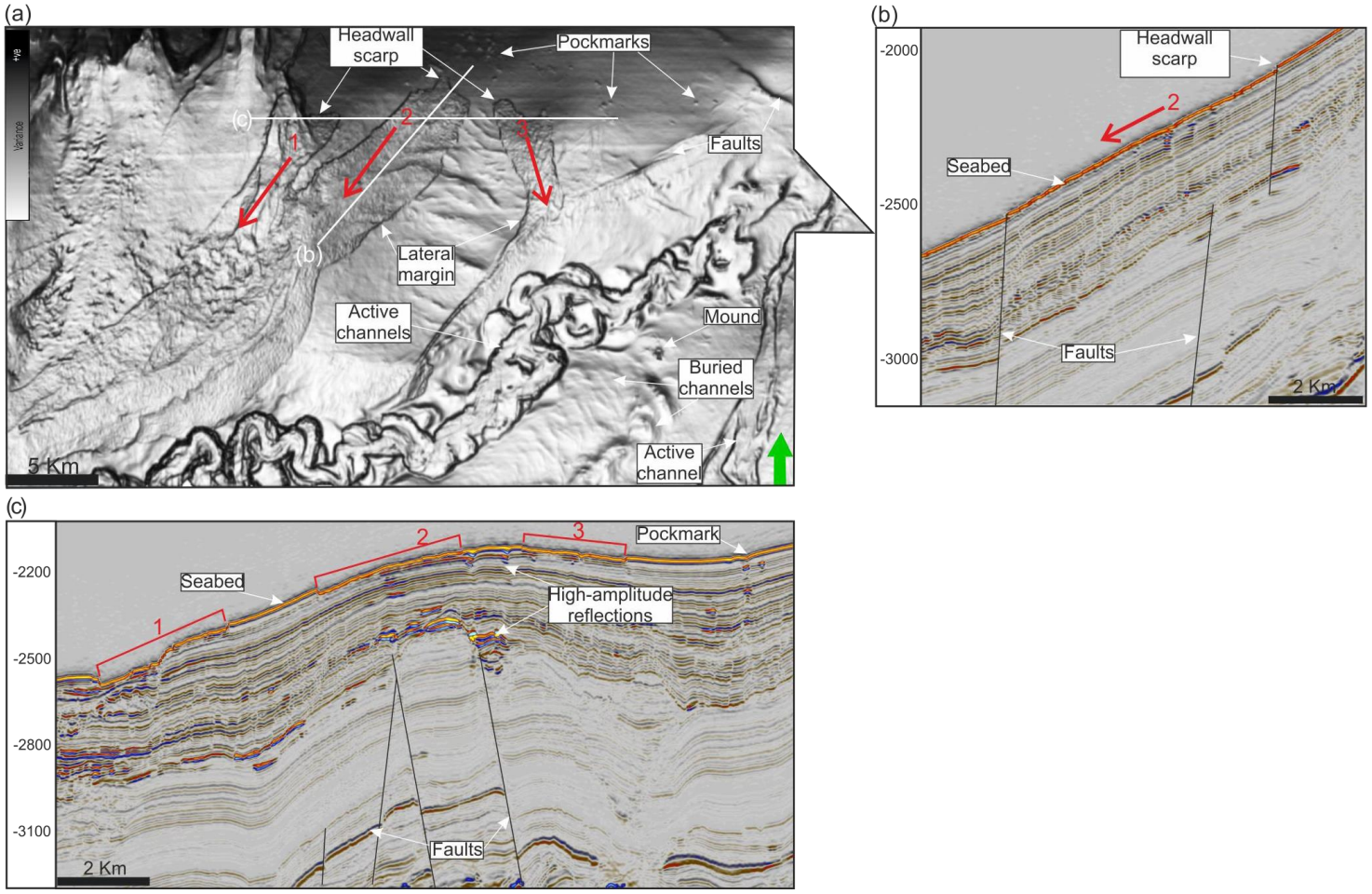

Fig 8.

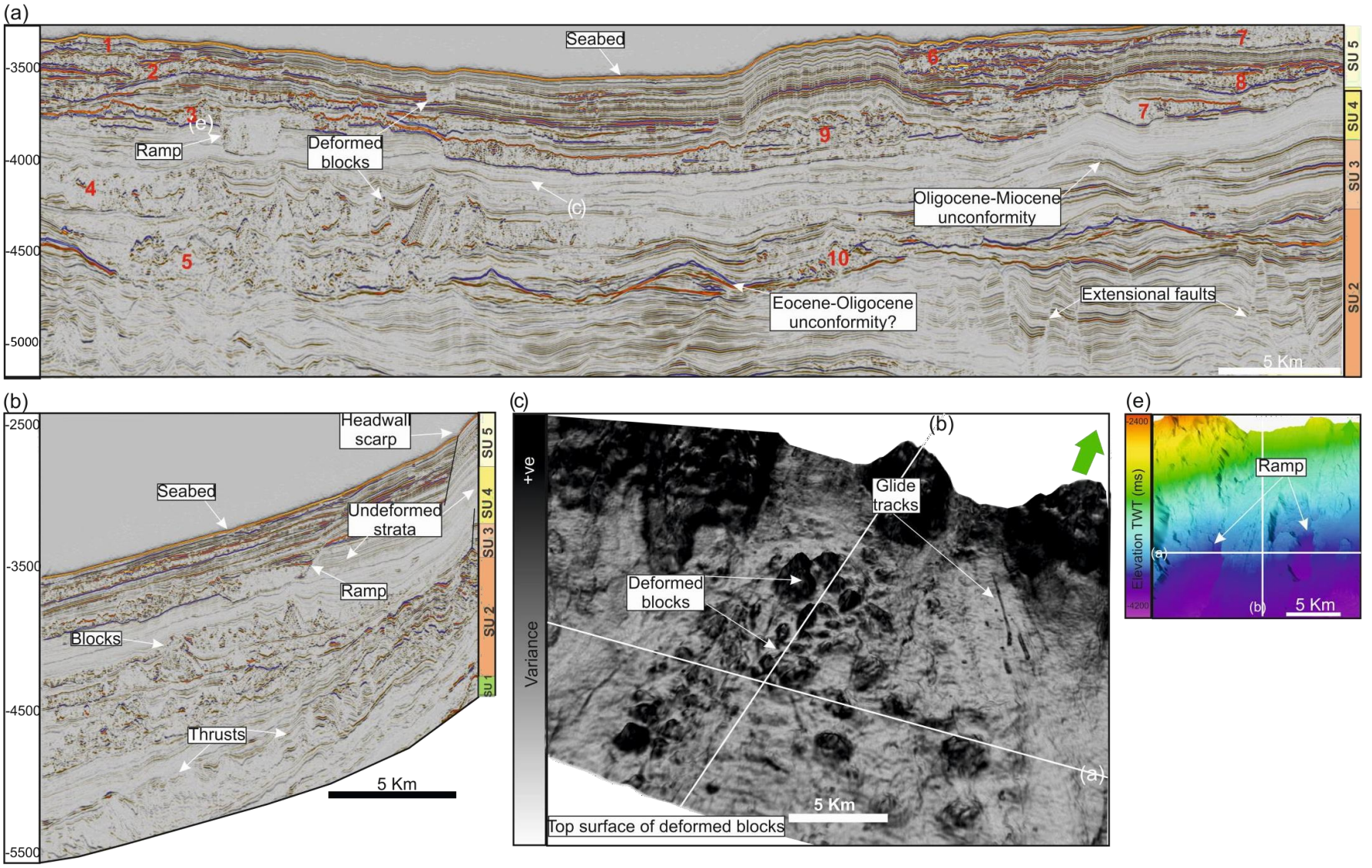
(a)
Seabed
Ramp
Deformed blocks
(c)
Oligocene-Miocene unconformity
Eocene-Oligocene unconformity?
Extensional faults
SU 5
SU 4
SU 3
SU 2
5 Km
(b)
Headwall scarp
Seabed
Undeformed strata
Ramp
Blocks
Thrusts
5 Km
(c)
+ve
Variance
(b)
Glide tracks
Deformed blocks
(a)
5 Km
Top surface of deformed blocks
(e)
Ramp
Elevation TWT (ms)
5 Km

Fig. 9.

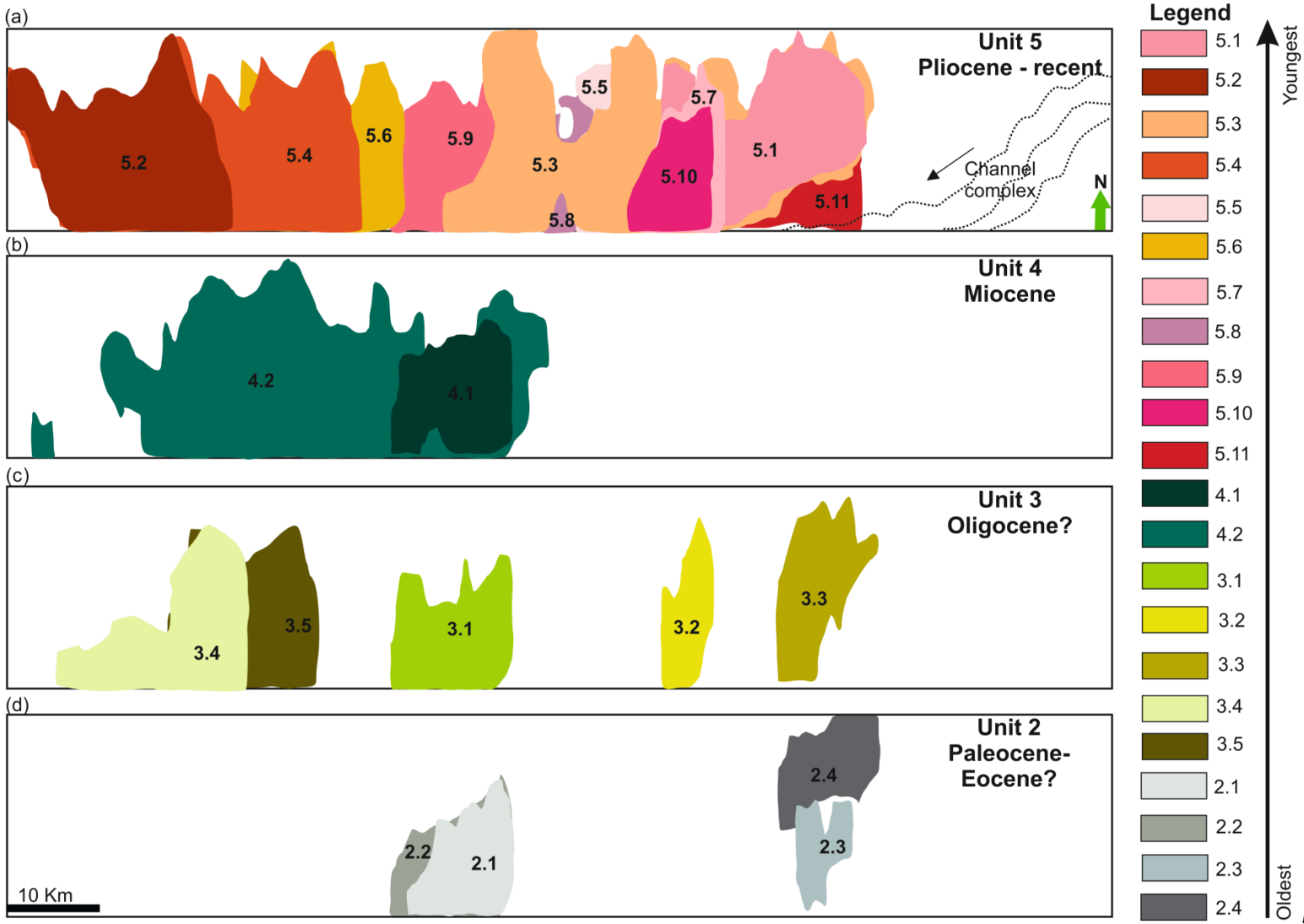
(a)
Unit 5
Pliocene - recent
5.2
5.4
5.6
5.9
5.3
5.5
5.7
5.10
5.1
5.11
5.8
Channel complex
N
(b)
Unit 4
Miocene
4.2
4.1
(c)
Unit 3
Oligocene?
3.4
3.5
3.1
3.2
3.3
(d)
Unit 2
Paleocene-Eocene?
2.2
2.1
2.4
2.3
10 Km
Legend
5.1
5.2
5.3
5.4
5.5
5.6
5.7
5.8
5.9
5.10
5.11
4.1
4.2
3.1
3.2
3.3
3.4
3.5
2.1
2.2
2.3
2.4
Youngest
Oldest

Fig. 10

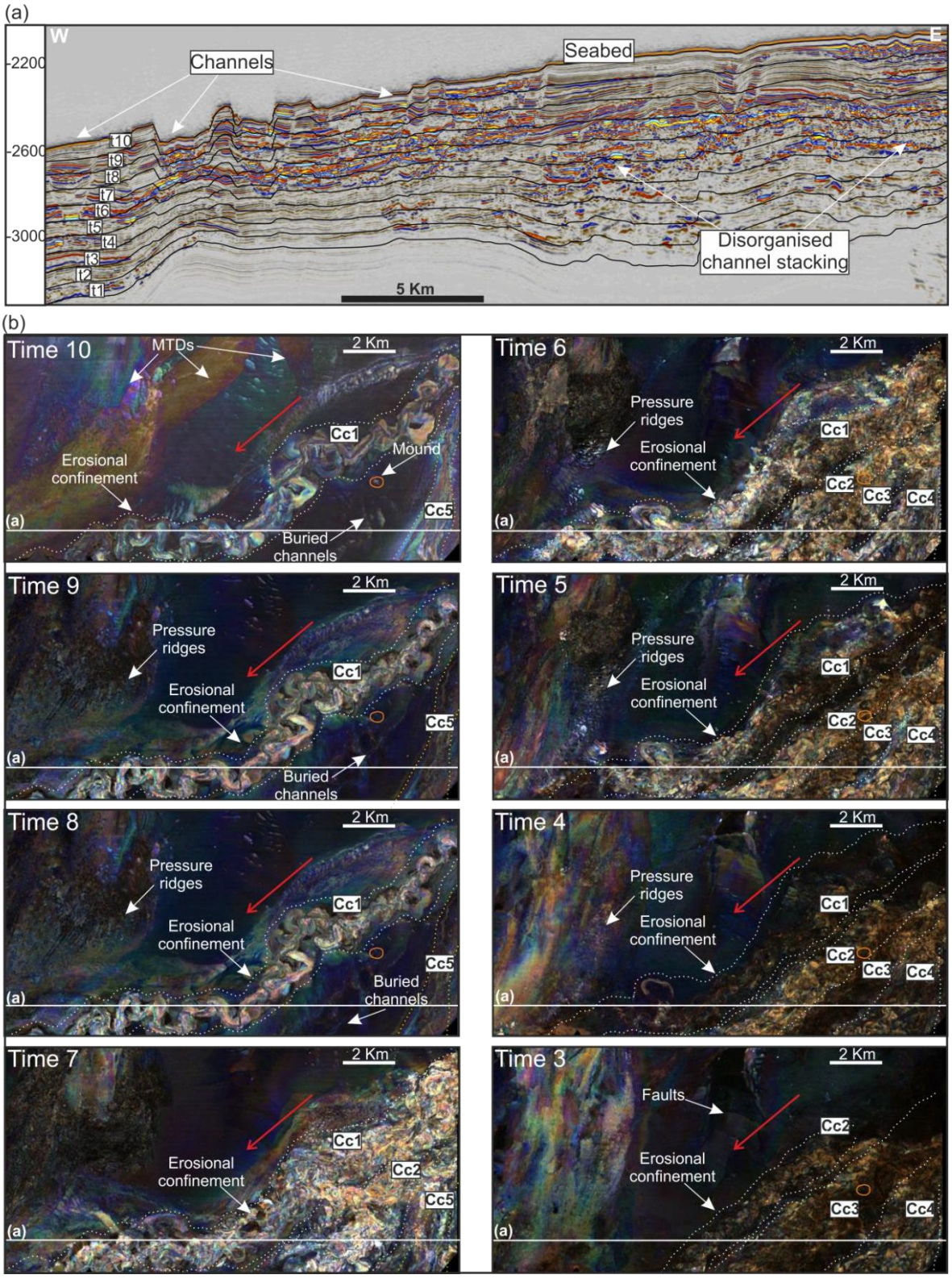
(a)
W
E
-2200
-2600
-3000
Channels
Seabed
t10
t9
t8
t7
t6
t5
t4
t3
t2
t1
Disorganised
channel stacking
5 Km
(b)
Time 10
MTDs
2 Km
Cc1
Mound
Erosional
confinement
Cc5
(a)
Buried
channels
Time 6
Pressure
ridges
Erosional
confinement
Cc1
Cc2
Cc3
Cc4
Time 9
Time 5
Time 8
Time 4
Time 7
Time 3
Faults

Fig 11.

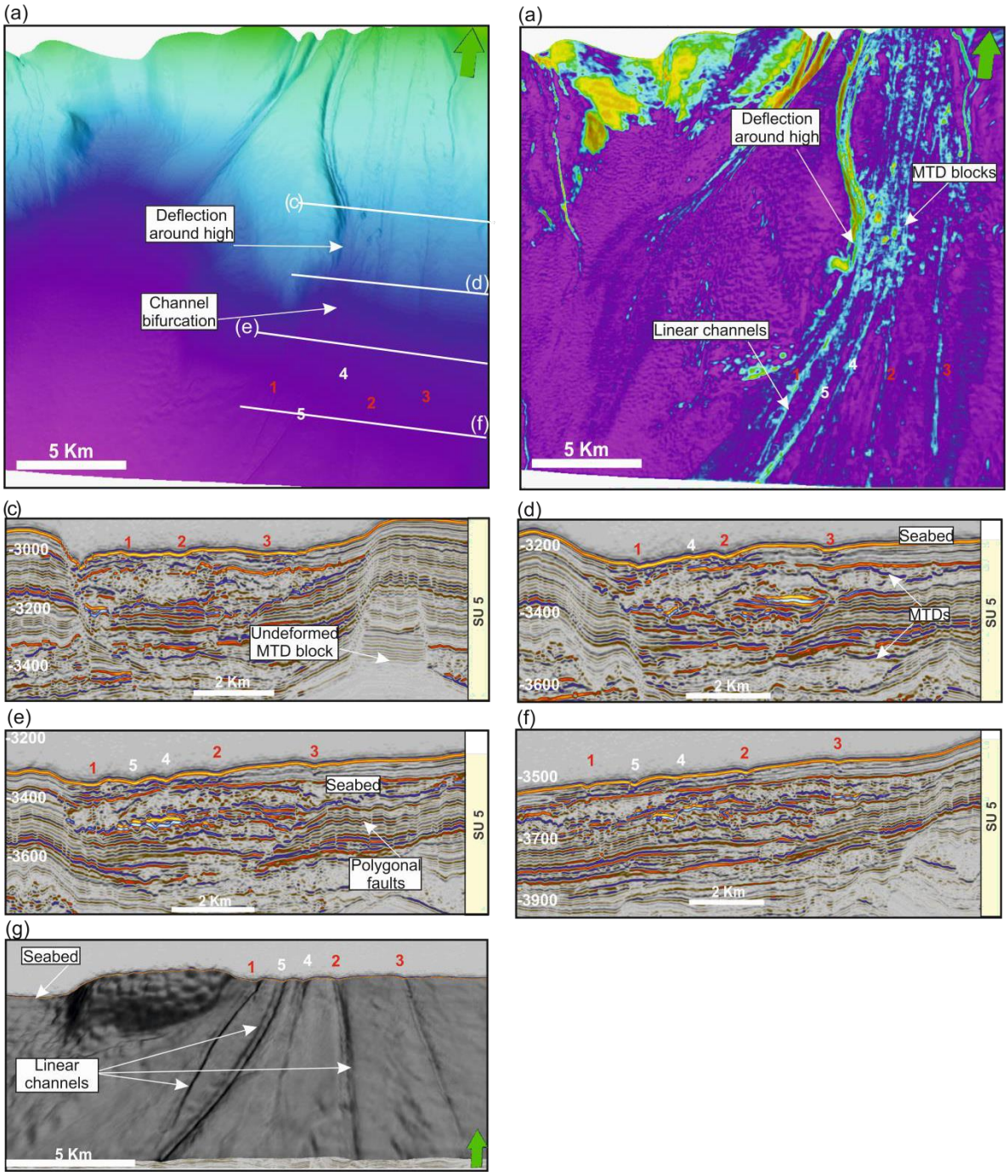
(a)
Deflection around high
(c)
(d)
Channel bifurcation
(e)
(f)
5 Km
(a)
Deflection around high
MTD blocks
Linear channels
5 Km
(c)
Undeformed MTD block
SU 5
2 Km
(d)
Seabed
MTDs
SU 5
2 Km
(e)
Seabed
Polygonal faults
SU 5
2 Km
(f)
SU 5
2 Km
(g)
Seabed
Linear channels
5 Km

Fig. 12

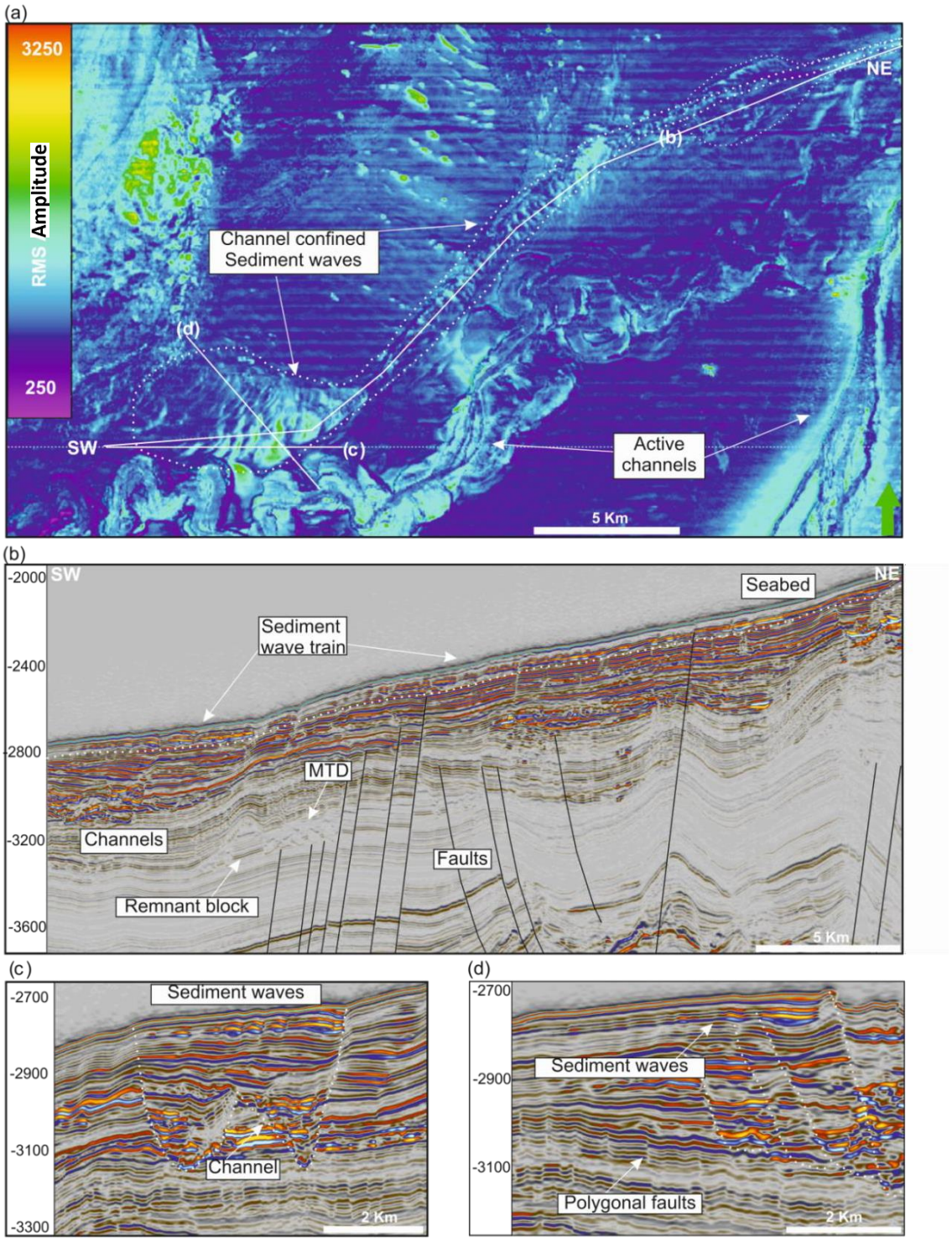
(a)
3250
RMS Amplitude
250
NE
(b)
Channel confined
Sediment waves
(d)
SW
(c)
Active
channels
5 Km
(b)
-2000
SW
Seabed
NE
Sediment
wave train
-2400
-2800
MTD
-3200
Channels
Faults
Remnant block
-3600
5 Km
(c)
(d)
-2700
Sediment waves
-2900
-3100
Channel
-3300
2 Km
-2700
Sediment waves
-2900
-3100
Polygonal faults
2 Km

Fig. 13.

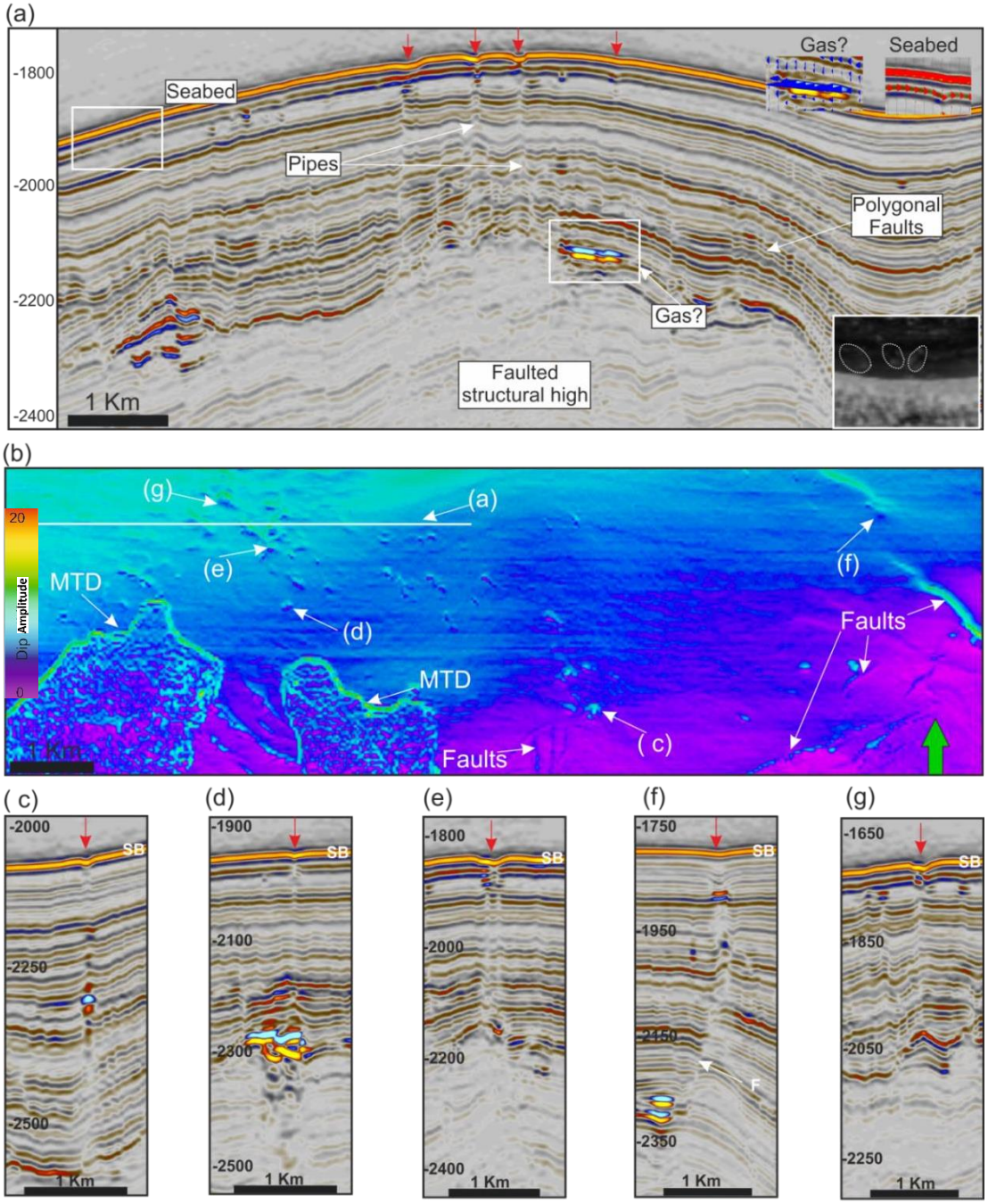
(a)
-1800
-2000
-2200
-2400
Seabed
Pipes
Gas?
Seabed
Polygonal Faults
Gas?
Faulted structural high
1 Km
(b)
20
Dip Amplitude
0
(g)
(a)
(e)
(f)
MTD
(d)
MTD
Faults
(c)
Faults
1 Km
(c)
-2000
SB
-2250
-2500
1 Km
(d)
-1900
SB
-2100
-2300
-2500
1 Km
(e)
-1800
SB
-2000
-2200
-2400
1 Km
(f)
-1750
SB
-1950
-2150
F
-2350
1 Km
(g)
-1650
SB
-1850
-2050
-2250
1 Km

Fig. 14.

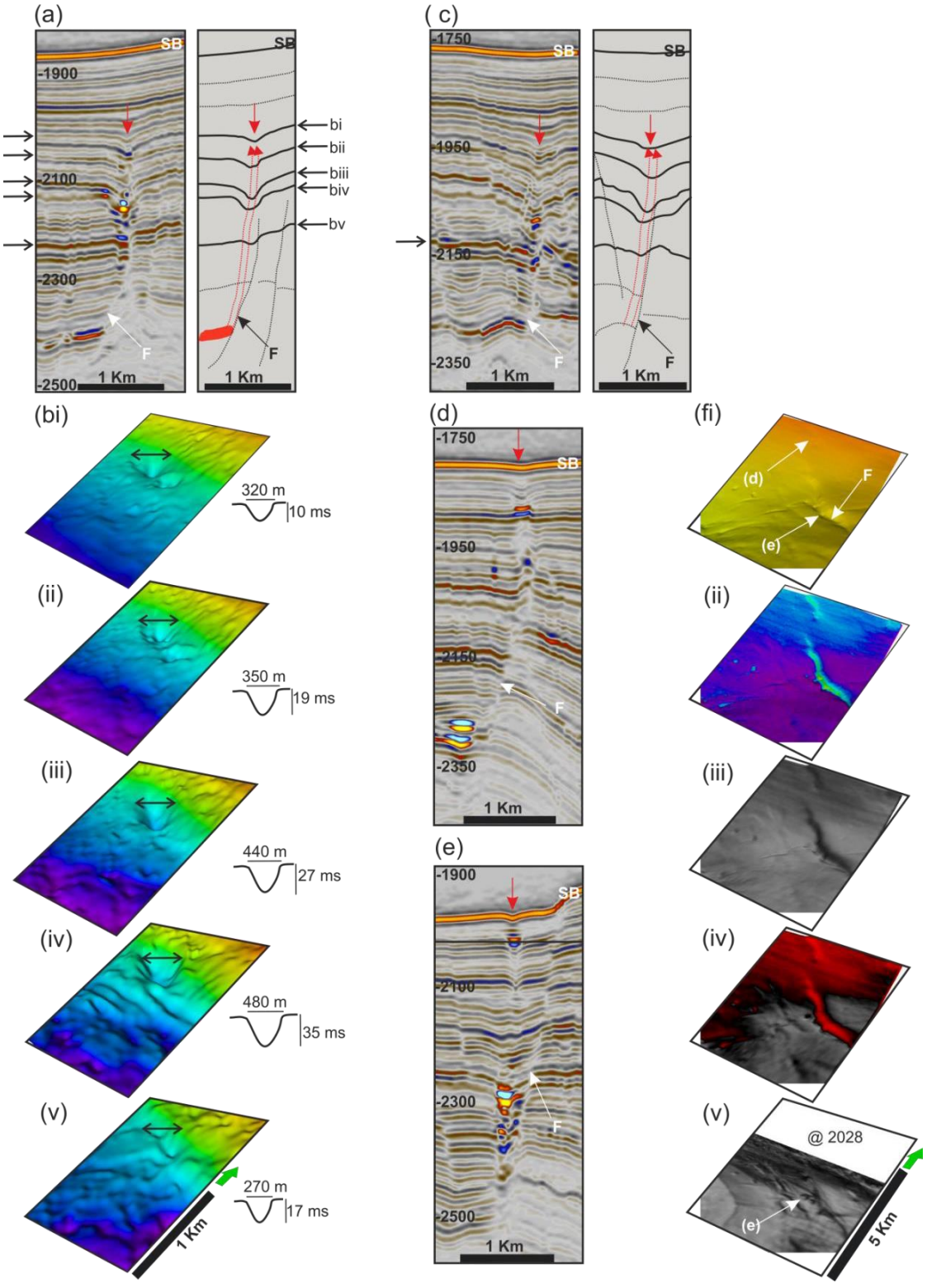
(a)
SB
-1900
-2100
-2300
-2500
F
1 Km
bi
bii
biii
biv
bv
(c)
-1750
-1950
-2150
-2350
(bi)
320 m
10 ms
(ii)
350 m
19 ms
(iii)
440 m
27 ms
(iv)
480 m
35 ms
(v)
270 m
17 ms
(d)
(e)
(fi)
@ 2028
5 Km

Fig.15.

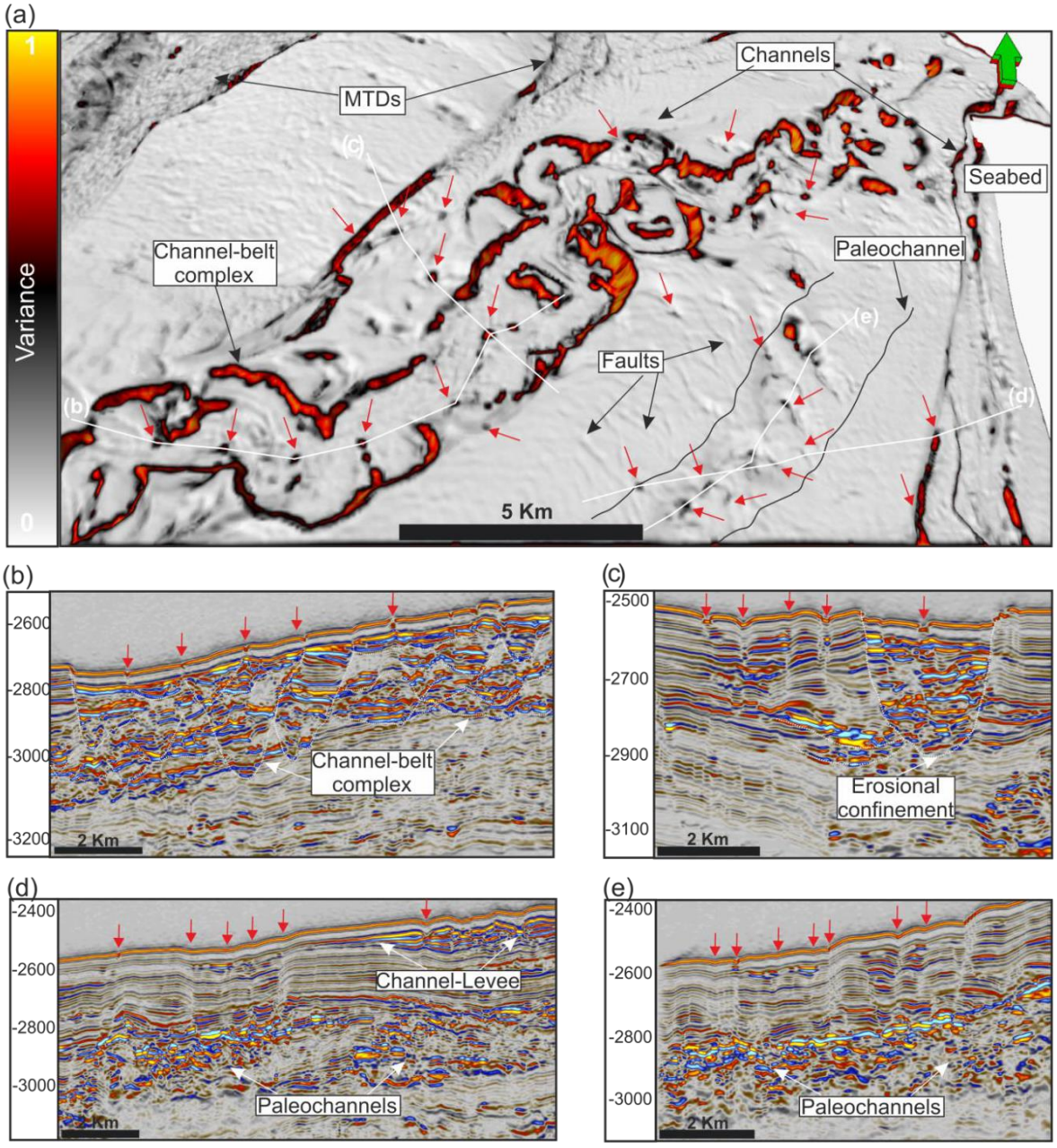
(a)
1
Variance
0
MTDs
Channels
Seabed
Channel-belt complex
Paleochannel
Faults
(b)
(c)
(d)
(e)
5 Km
(b)
-2600
-2800
-3000
-3200
Channel-belt complex
2 Km
(c)
-2500
-2700
-2900
-3100
Erosional confinement
2 Km
(d)
-2400
-2600
-2800
-3000
Channel-Levee
Paleochannels
2 Km
(e)
-2400
-2600
-2800
-3000
Paleochannels
2 Km

Fig. 16

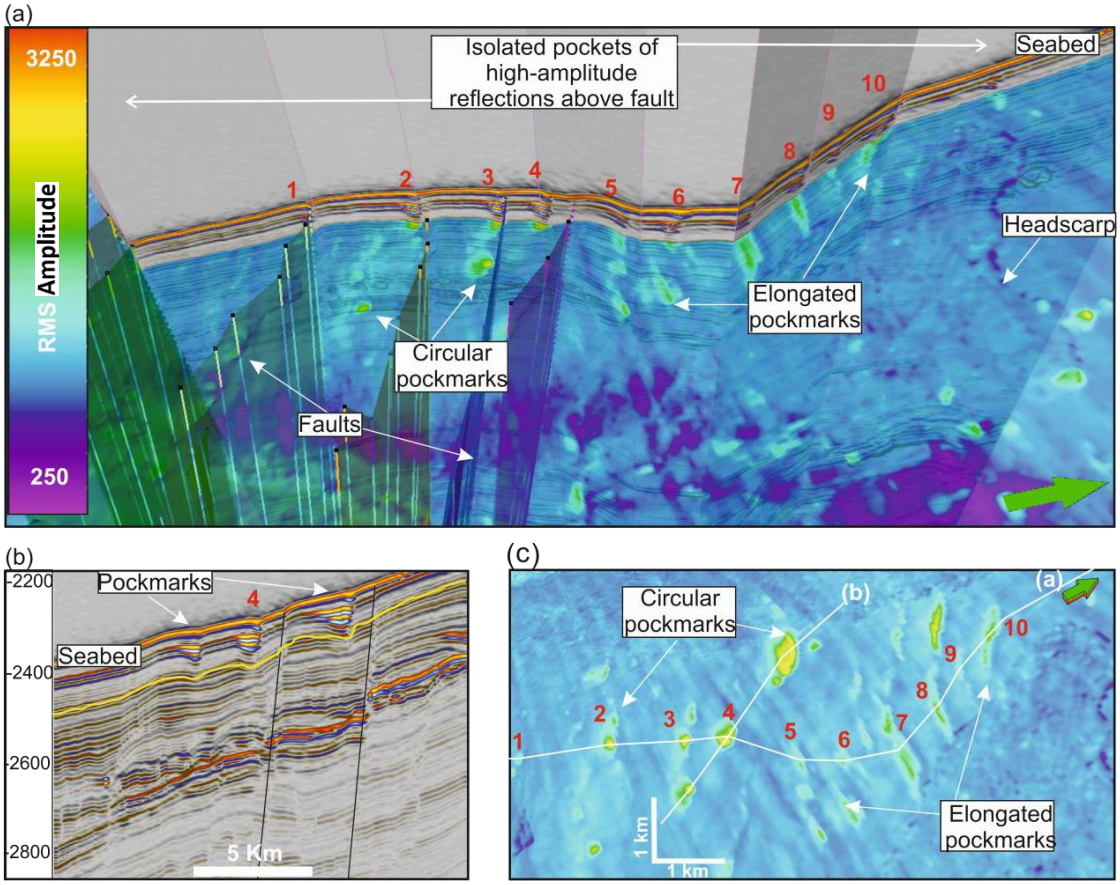
(a)
3250
RMS Amplitude
250
Isolated pockets of high-amplitude reflections above fault
Seabed
Headscarp
Elongated pockmarks
Circular pockmarks
Faults
(b)
Pockmarks
Seabed
5 Km
(c)
Circular pockmarks
Elongated pockmarks
1 km
1 km

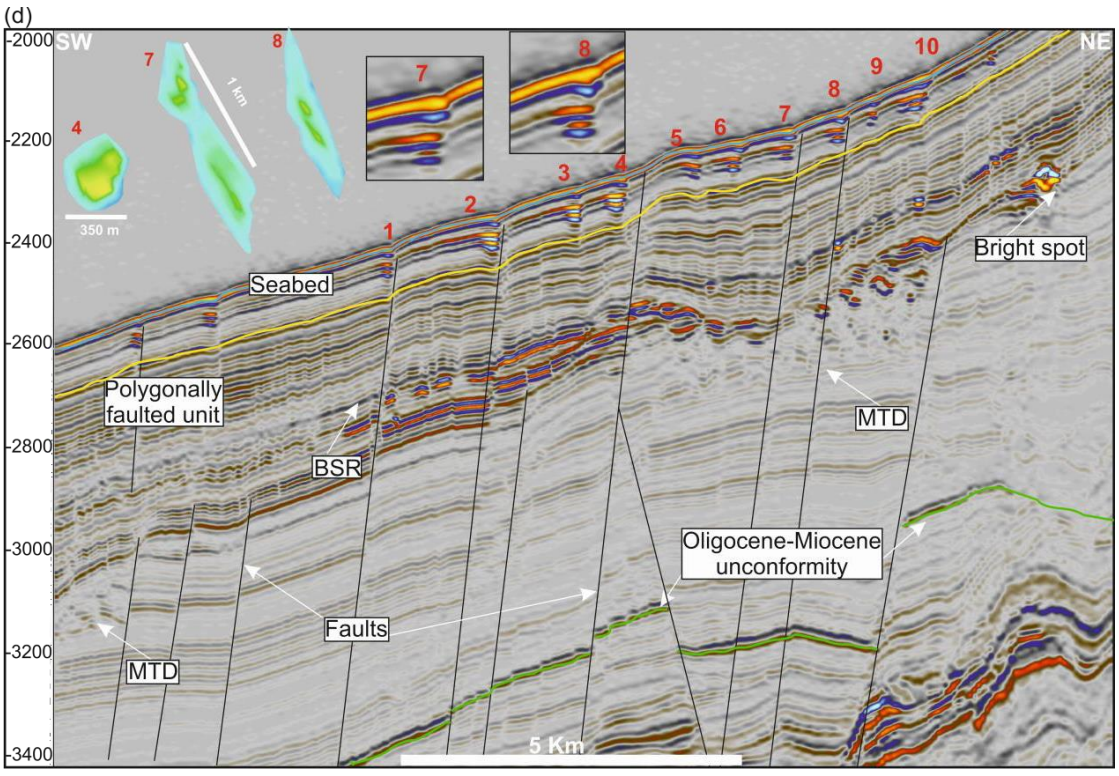
(d)
SW
NE
350 m
1 km
Seabed
Polygonally faulted unit
BSR
Faults
MTD
MTD
Bright spot
Oligocene-Miocene unconformity
5 Km

Fig. 17

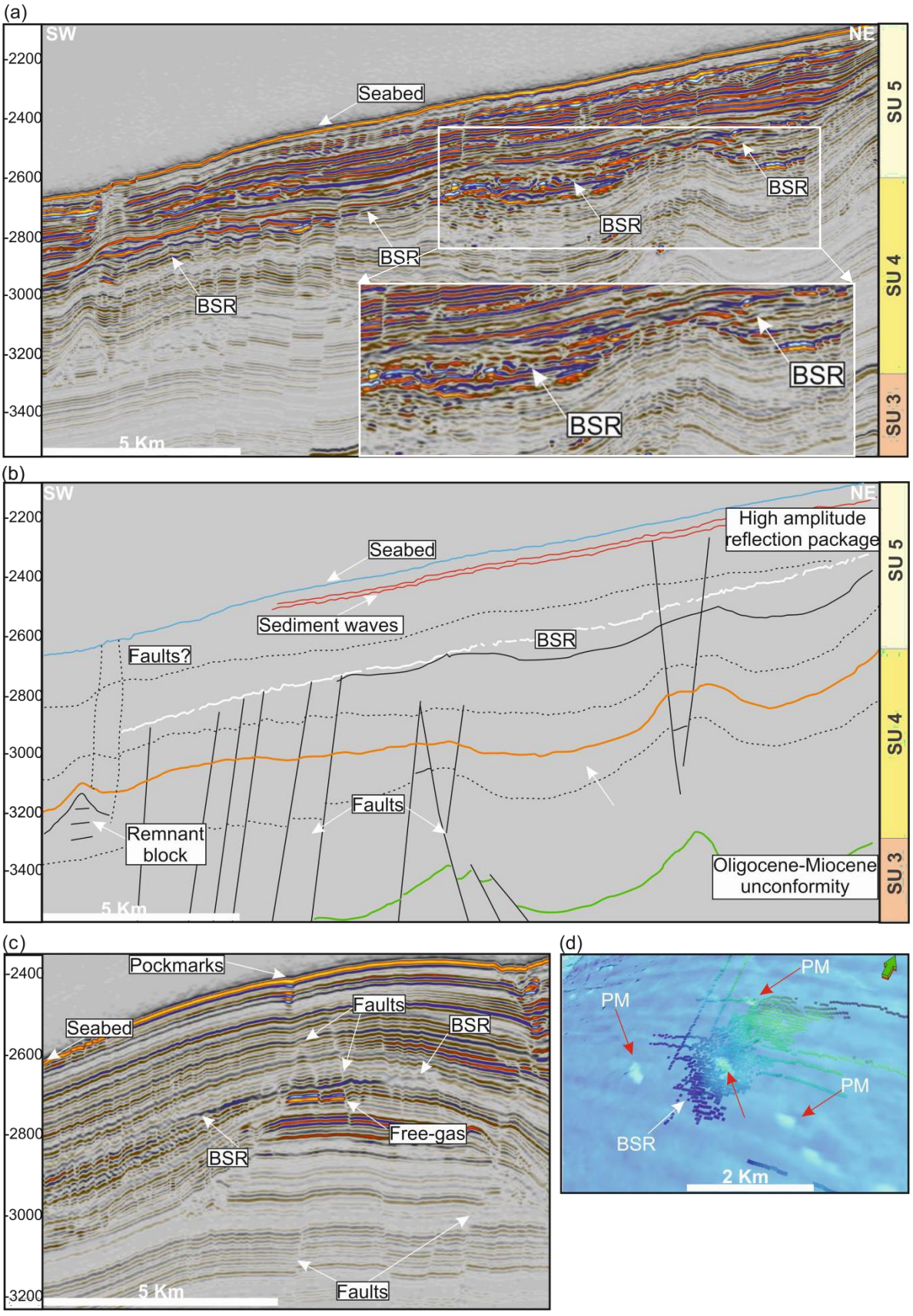
(a)
SW
NE
-2200
-2400
-2600
-2800
-3000
-3200
-3400
Seabed
BSR
BSR
BSR
BSR
BSR
BSR
5 Km
SU 5
SU 4
SU 3
(b)
SW
NE
-2200
-2400
-2600
-2800
-3000
-3200
-3400
High amplitude reflection package
Seabed
Sediment waves
BSR
Faults?
Faults
Remnant block
Oligocene-Miocene unconformity
5 Km
SU 5
SU 4
SU 3
(c)
-2400
-2600
-2800
-3000
-3200
Pockmarks
Seabed
Faults
BSR
Free-gas
BSR
Faults
5 Km
(d)
PM
PM
PM
BSR
2 Km

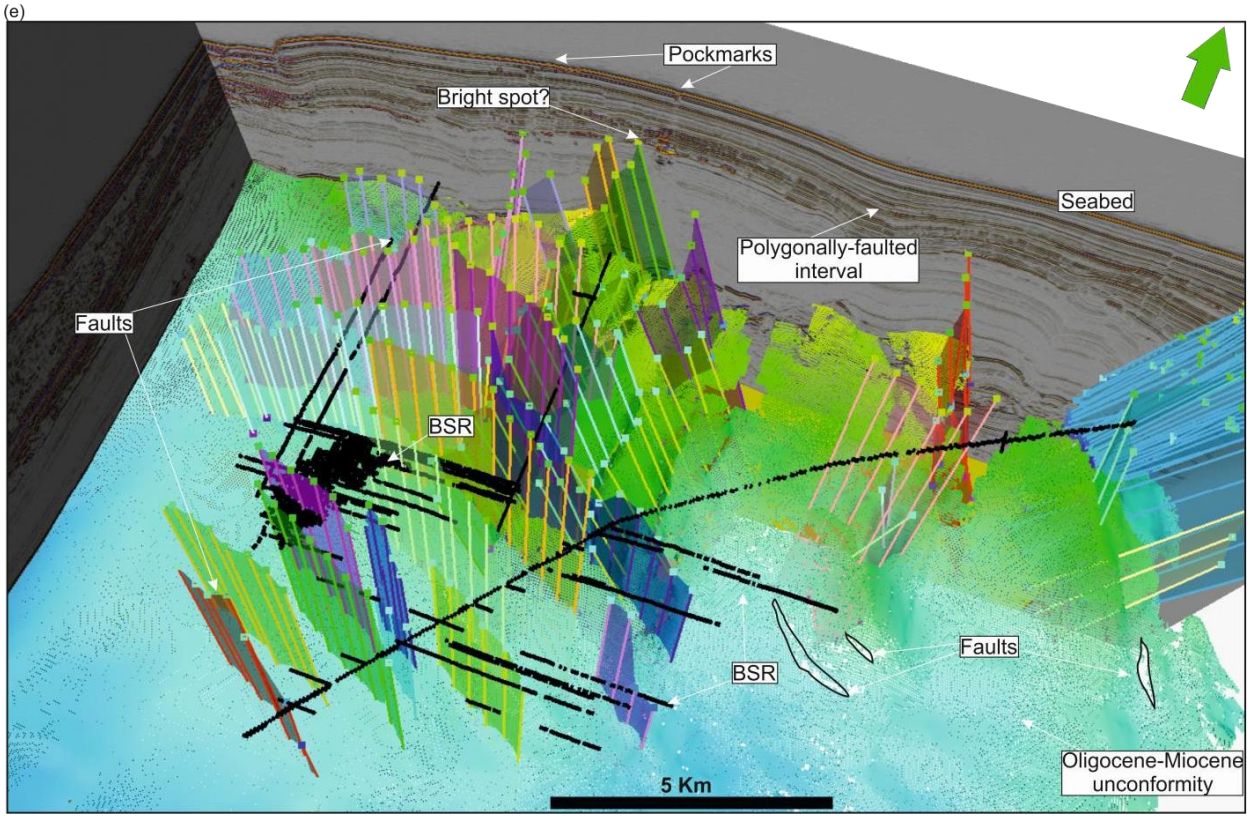
(e)
Pockmarks
Bright spot?
Seabed
Polygonally-faulted interval
Faults
BSR
BSR
Faults
Oligocene-Miocene unconformity
5 Km

Fig. 18

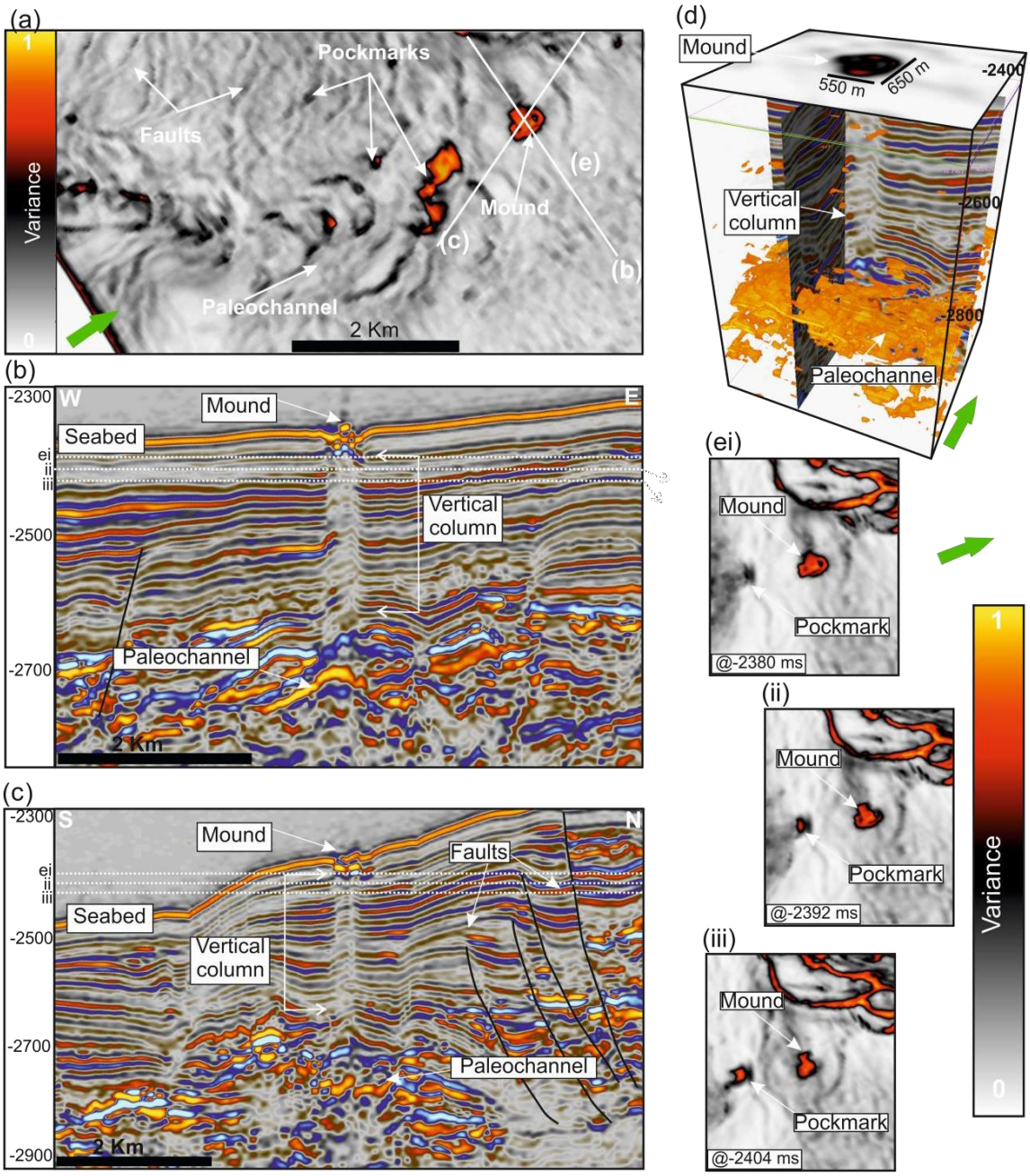
(a)
Variance
1
0
Pockmarks
Faults
(e)
Mound
(c)
(b)
Paleochannel
2 Km
(b)
-2300
W
E
Mound
Seabed
ei
ii
iii
-2500
Vertical column
-2700
Paleochannel
2 Km
(c)
-2300
S
N
Mound
Faults
ei
ii
iii
Seabed
-2500
Vertical column
-2700
Paleochannel
2 Km
-2900
(d)
Mound
550 m
650 m
-2400
Vertical column
-2600
-2800
Paleochannel
(ei)
Mound
Pockmark
@-2380 ms
(ii)
Mound
Pockmark
@-2392 ms
(iii)
Mound
Pockmark
@-2404 ms
1
Variance
0

Fig.19.

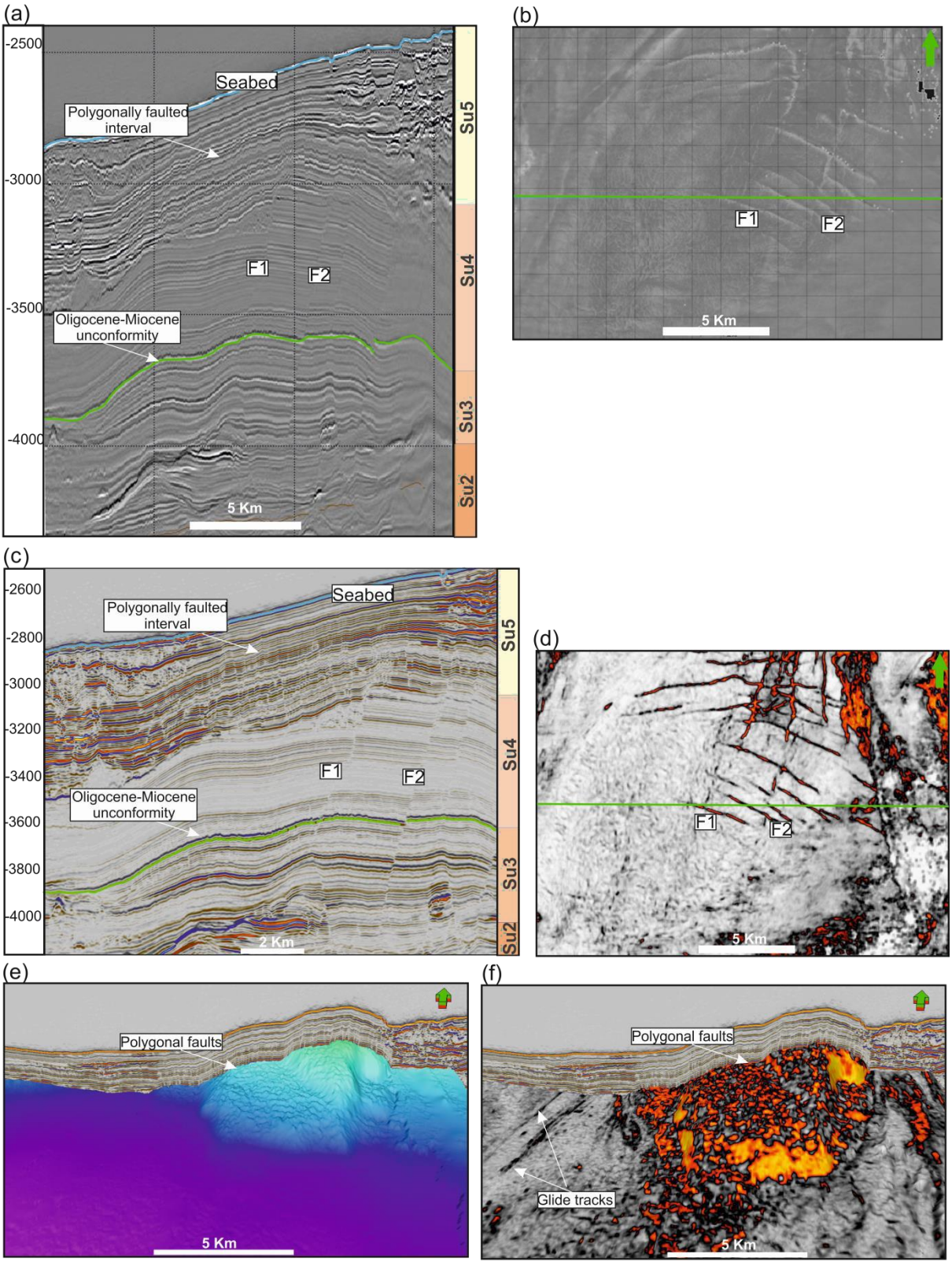
(a)
-2500
-3000
-3500
-4000
Seabed
Polygonally faulted interval
F1
F2
Oligocene-Miocene unconformity
Su5
Su4
Su3
Su2
5 Km
(b)
F1
F2
5 Km
(c)
-2600
-2800
-3000
-3200
-3400
-3600
-3800
-4000
Seabed
Polygonally faulted interval
F1
F2
Oligocene-Miocene unconformity
Su5
Su4
Su3
Su2
2 Km
(d)
F1
F2
5 Km
(e)
Polygonal faults
5 Km
(f)
Polygonal faults
Glide tracks
5 Km

Fig 20.

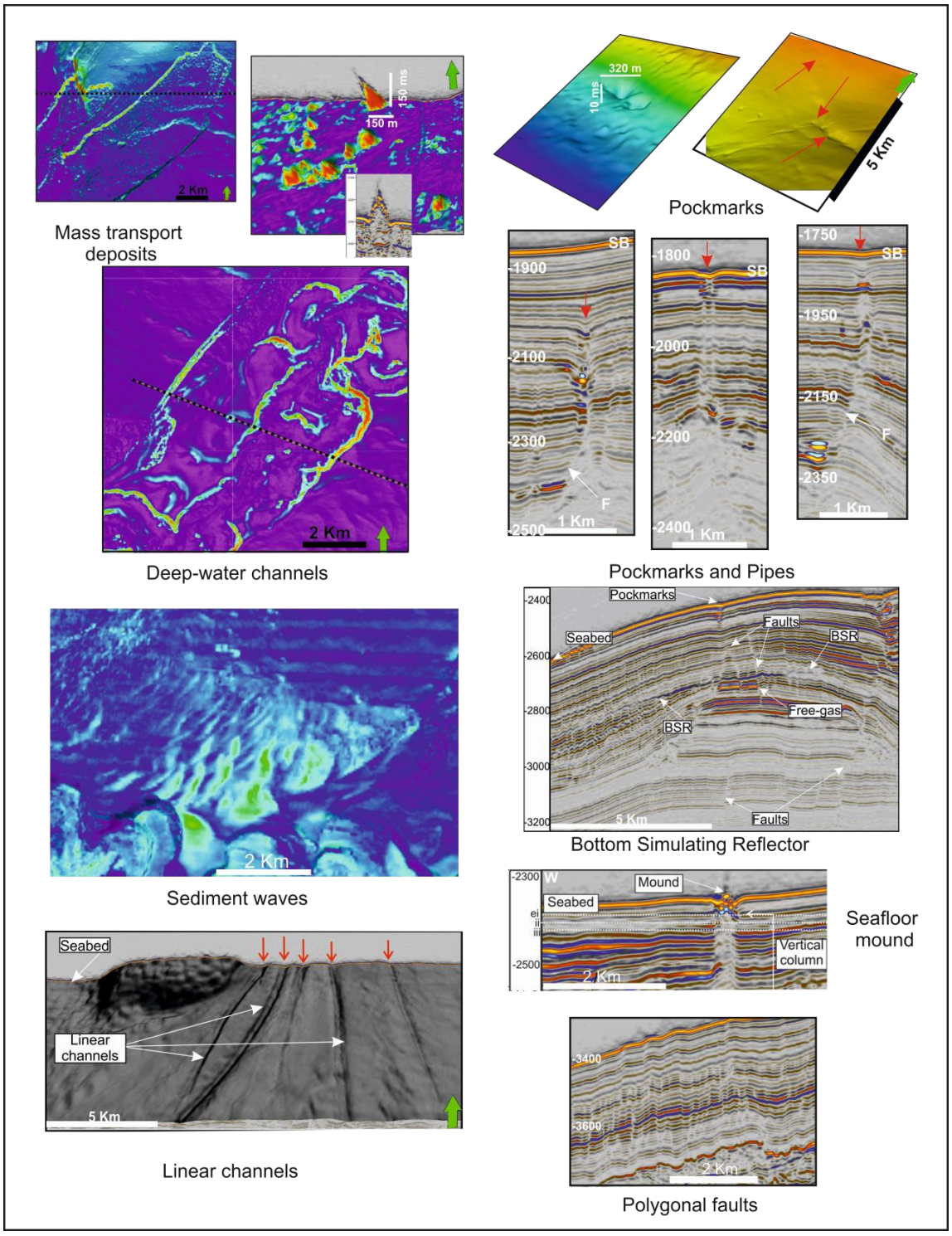
2 Km
150 m
150 ms
Mass transport deposits
320 m
10 ms
5 Km
Pockmarks
SB
-1900
-2100
-2300
-2500
F
1 Km
-1800
-2000
-2200
-2400
-1750
-1950
-2150
-2350
Pockmarks and Pipes
2 Km
Deep-water channels
Pockmarks
Seabed
Faults
BSR
Free-gas
-2400
-2600
-2800
-3000
-3200
5 Km
Bottom Simulating Reflector
2 Km
Sediment waves
-2300
W
Mound
Seabed
ei
ii
iii
-2500
Vertical column
Seafloor mound
Seabed
Linear channels
5 Km
Linear channels
-3400
-3600
Polygonal faults

Fig. 21

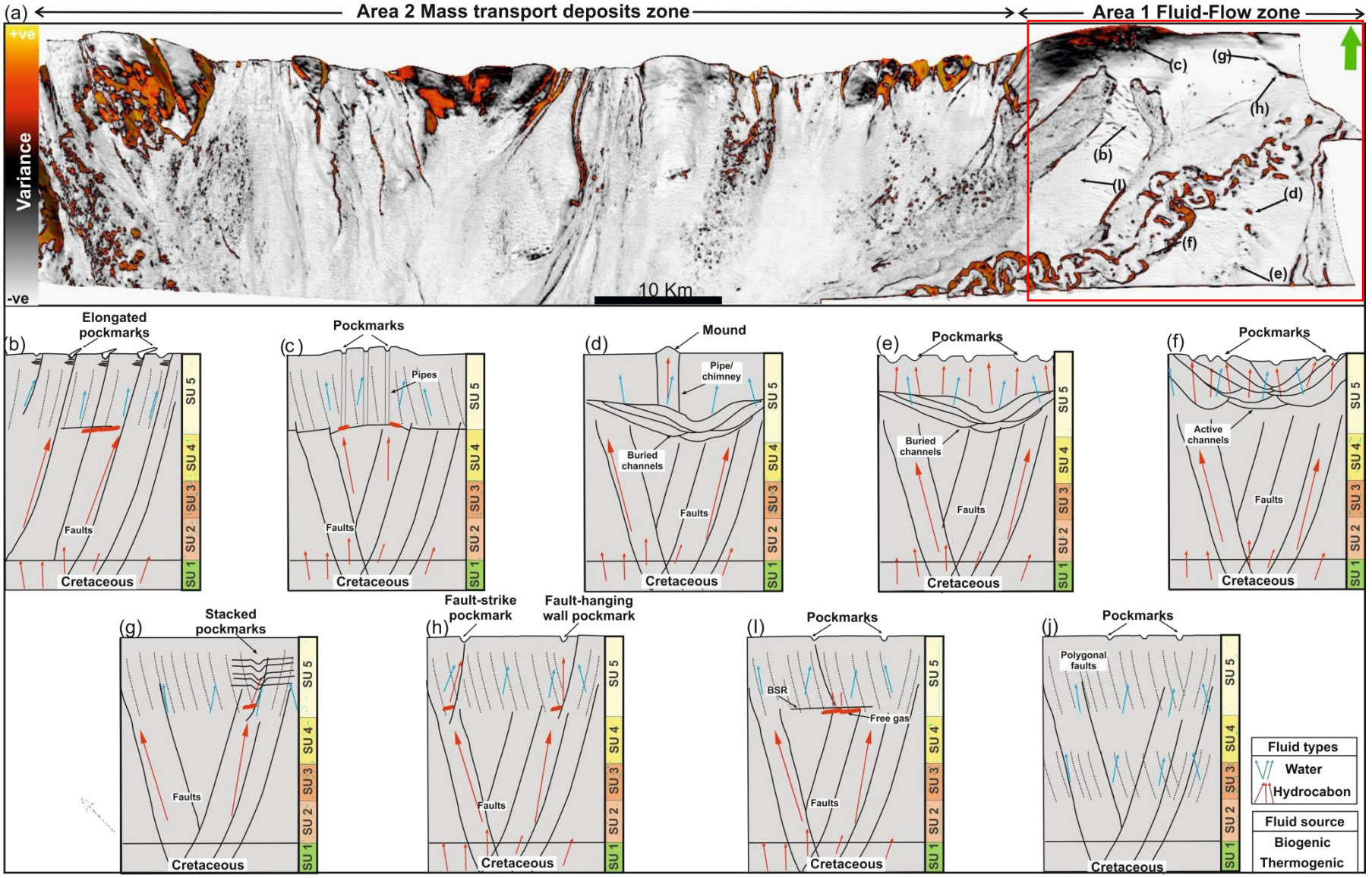
(a)
Area 2 Mass transport deposits zone
Area 1 Fluid-Flow zone
+ve
Variance
-ve
10 Km
(b)
(c)
(d)
(e)
(f)
(g)
(h)
(l)
(j)
Elongated pockmarks
Pockmarks
Pipes
Mound
Pipe/ chimney
Buried channels
Active channels
Stacked pockmarks
Fault-strike pockmark
Fault-hanging wall pockmark
BSR
Free gas
Polygonal faults
Faults
Cretaceous
SU 1
SU 2
SU 3
SU 4
SU 5
Fluid types
Water
Hydrocabon
Fluid source
Biogenic
Thermogenic

Fig. 22

Fig22a inset

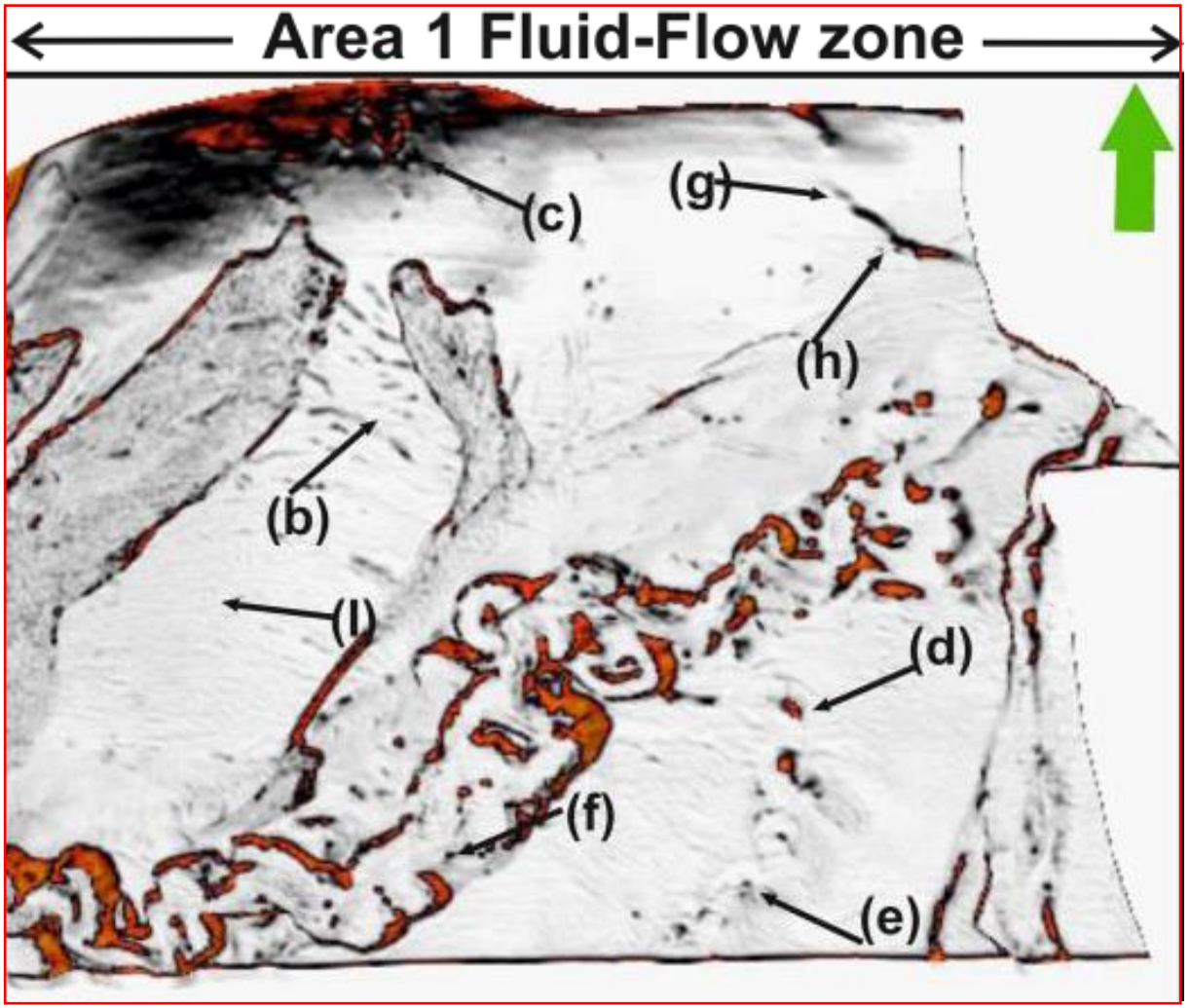

Fig22a inset

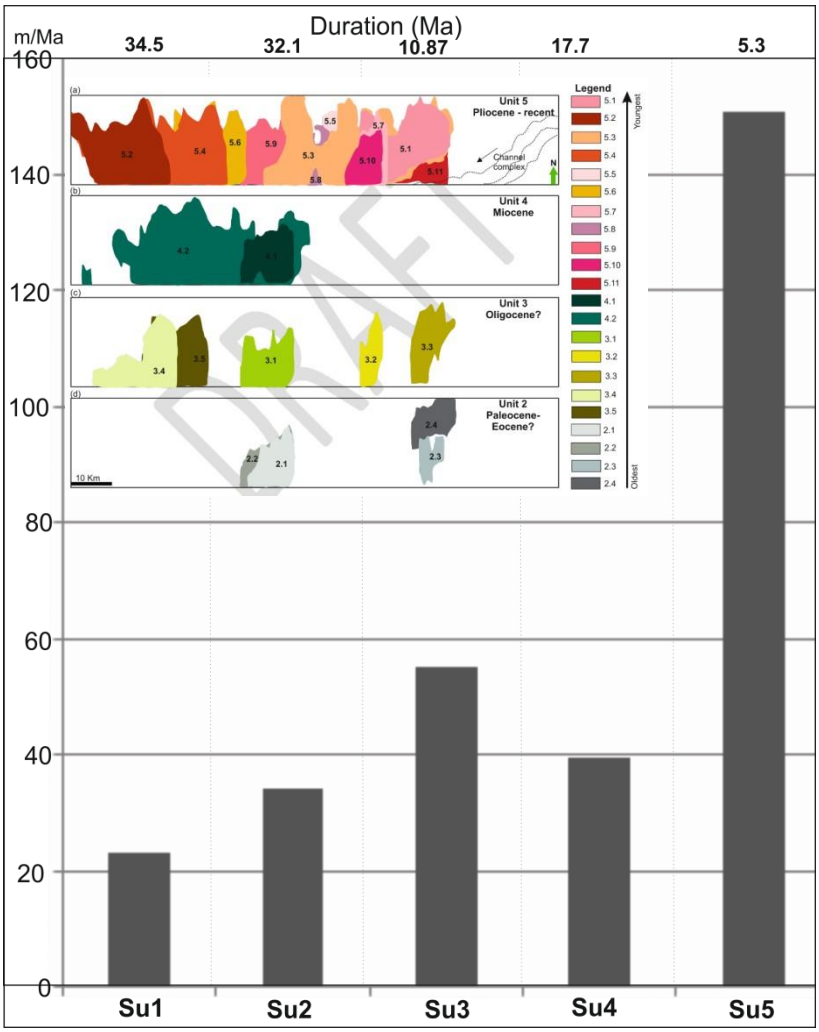
Duration (Ma)
m/Ma
34.5
32.1
10.87
17.7
5.3
160
140
120
100
80
60
40
20
0
Unit 5
Pliocene - recent
Unit 4
Miocene
Unit 3
Oligocene?
Unit 2
Paleocene-
Eocene?
Channel complex
N
10 Km
Legend
Youngest
Oldest
Su1
Su2
Su3
Su4
Su5

Fig. 23

SEISMIC UNITS	FREQUENCY (hz)	INTERVAL VELOCITIES (km/s)	HORIZONTAL RESOLUTION (m)	VERTICAL RESOLUTION (m)
SU1	25	2	42	20
SU2	48	2	21	10
SU3	30	2	33	17
SU4	40	2	25	13
SU5	50	2	20	10

Table 1

BASIN EXAMPLE	2D GEOMETRY	PLAN VIEW GEOMETRY	FAULT THROW (M)	RANGE/AV FAULT DIP (º)	AUTHORS
Central North Sea	Normal faults	Distinctly Polygonal	NA	30 – 70 (45)	Cartwright & Lonergan 1996
Central North Sea	Normal faults	Distinctly Polygonal	8 – 100	27 – 67 (45)	Lonergan *et al.,* 1998
Northern North Sea	Normal faults	Distinctly Polygonal	8 – 30	31 – 56	Olobayo *et al.,* 2015
Faroe-Shetland Basin	Normal faults	Distinctly Polygonal	NA	55 – 85 (58 +/-2)	Shoulders *et al.,* 2007
Faroe-Shetland Basin	Normal faults	Distinctly Polygonal	NA	Type 2a – 63 Type 3 - 68	Bureau *et al.,* 2013
More Basin	Normal faults	Distinctly Polygonal	Few metres to 80	25 - 50	Stuevold *et al.,* 2003
Lower Congo Basin	Normal faults	Distinctly Polygonal	5 - 20	NA	Gay *et al.,* 2004
Nigeria Transform Margin	**Normal faults**	**Slightly polygonal**	**3-11**	**41 – 50 (46)**	**This study**

Table 2

SEISMIC UNITS	SERIES	DURATION (Ma)	THICKNESS (ms) max	VELOCITY (Km/s)	NET ACC. RATE (m/Ma) max
SU1	Late Cretaceous	34.5	800	2	23.2
SU2	Paleocene-Eocene?	32.1	1100	2	34.3
SU3	Oligocene?	10.87	700	2	55.2
SU4	Miocene?	17.7	900	2	39.5
SU5	Pliocene to date?	5.3	1100	2	150.9

Table 3